Flow induced by the rotation of two circular cylinders in a viscous fluid

E. Dormy ●[1] and H. K. Moffatt ●[2]

[1]*Département de Mathématiques et Applications, UMR-8553, École Normale Supérieure,
CNRS, PSL University, 75005 Paris, France*
[2]*Department of Applied Mathematics and Theoretical Physics, Wilberforce Road,
Cambridge CB3 0WA, United Kingdom*

The low-Reynolds-number Stokes flow driven by rotation of two parallel cylinders of equal unit radius is investigated by both analytical and numerical techniques. In Part I, the case of counterrotating cylinders is considered. A numerical (finite-element) solution is obtained by enclosing the system in an outer cylinder of radius $R_0 \gg 1$, on which the no-slip condition is imposed. A model problem with the same symmetries is first solved exactly, and the limit of validity of the Stokes approximation is determined; this model has some relevance for ciliary propulsion. For the two-cylinder problem, attention is focused on the small-gap situation $\varepsilon \ll 1$. An exact analytic solution is obtained in the contact limit $\varepsilon = 0$, and a net force F_c acting on the pair of cylinders in this contact limit is identified; this contributes to the torque that each cylinder experiences about its axis. The far-field torque doublet ("torquelet") is also identified. Part II treats the case of corotating cylinders, for which again a finite-element numerical solution is obtained for $R_0 \gg 1$. The theory of Watson [Mathematika **42**, 105 (1995)] is elucidated and shown to agree well with the numerical solution. In contrast to the counterrotating case, inertia effects are negligible throughout the fluid domain, however large, provided Re $\ll 1$. In the concluding section, the main results for both cases are summarized, and the situation when the fluid is unbounded ($R_0 = \infty$) is discussed. If the cylinders are free to move (while rotating about their axes), in the counterrotating case they will then translate relative to the fluid at infinity with constant velocity, the drag force exactly compensating the self-induced force due to the counterrotation. In the corotating case, if the cylinders are free to move, then they will rotate as a pair relative to the fluid at infinity and the net torque on the cylinder pair is zero; the flow relative to the fluid at infinity is identified as a "radial quadrupole." If, however, the cylinder axes are held fixed, then the Stokes flow in the counterrotating case extends only for a distance $r \sim \mathrm{Re}^{-1} \log [\mathrm{Re}^{-1}]$ from the cylinders, and it is argued that the cylinders then experience a (dimensionless) force $\hat{F}_y \sim 1/ \log [\mathrm{Re}^{-1} \log [\mathrm{Re}^{-1}]]$; in the corotating case, the cylinder pair experiences a (dimensionless) torque $\hat{\mathcal{T}}$, which tends to 17.2587 as $\varepsilon \downarrow 0$; this torque is associated with a vortex-type flow $\sim r^{-1}$ that is established in the far field. Situations that can be described by the condition $\varepsilon < 0$ are treated for both counter- and corotating cases in the Supplemental Material.

INTRODUCTION

The very classical problem of determining the two-dimensional flow induced by the rotation of two adjacent cylinders of equal unit radii originated with the pioneering work of Jeffery [1,2]. Jeffery's solution involved a velocity field that failed to tend to zero at infinity ("Jeffery's paradox"). Our motivation in the present study is to understand how this paradox may be resolved. The cases of counterrotating or corotating cylinders are very different and are treated separately in Parts I

and II below. In both cases, we circumvent the condition of "zero velocity at infinity" by enclosing the fluid in a cylinder of large radius $R_0 \gg 1$, on which a no-slip condition may be imposed. We then seek to infer the behavior in the limiting situation when the fluid is unbounded ($R_0 = \infty$). Important applications are to be found in the theory of swimming microorganisms as treated in the book of Lauga [3], or in the behavior and interaction of two-dimensional microswimmers, as studied recently by Nie *et al.* [4].

We pay particular attention to the situation when the gap 2ε between the cylinders is small. The combination of conditions $R_0 \gg 1$ and $\varepsilon \ll 1$ is numerically challenging, but we can exploit lubrication theory in the small gap and check the accuracy and range of applicability of the finite-element numerical scheme that is adopted. The problem studied here is prototypical, in that our approach may be extended to a range of problems in either two or three dimensions where the topology is nontrivial and small gaps (or contact) between moving solid bodies may occur.

PART I: COUNTERROTATING CYLINDERS

A. Background

The problem of determining the two-dimensional steady Stokes flow induced by the counter-rotation of two parallel cylinders of infinite length in an unbounded viscous fluid was initiated in the seminal work of Jeffery [2]. The symmetries of the streamline patterns (the angular velocities being equal and opposite) are as indicated in Fig. 1. Using bipolar coordinates and conformal transformation, Jeffery showed that it was not possible to satisfy the condition that the fluid velocity should vanish at infinity ("Jeffery's paradox"). He did however find a solution that allowed for a uniform streaming flow at infinity. (The situation is in some respects like the classical problem of viscous flow past a circular cylinder, for which Stokes had himself established that there is no solution of the linearized equations satisfying the required condition at infinity [5,6]; this difficulty was ultimately resolved by Proudman and Pearson [7] through the (then novel) technique of matched asymptotic expansions.) For ease of reference, some aspects of Jeffery's approach are summarized in Appendix A, together with a new asymptotic evaluation of his results.

We use dimensionless variables such that the two cylinders $\mathcal{C}_{1,2}$ have equal unit radius $a = 1$, are centered at $(\mp(1 + \varepsilon), 0)$, and rotate with angular velocities $\Omega_1 = 1$, $\Omega_2 = -1$, respectively; the no-slip condition is to be satisfied on both cylinders. The natural Reynolds number for the problem is then

$$\text{Re} = \Omega_1 a^2/\nu = \nu^{-1}, \tag{1}$$

where ν is the kinematic viscosity in dimensionless units. The gap between the cylinders is 2ε, and their boundaries are

$$\mathcal{C}_1 : (x + 1 + \varepsilon)^2 + y^2 = 1 \quad \text{and} \quad \mathcal{C}_2 : (x - 1 - \varepsilon)^2 + y^2 = 1. \tag{2}$$

We shall be particularly concerned with the "small-gap situation," $0 < \varepsilon \ll 1$. In the limiting situation $\varepsilon = 0$, the cylinders make contact and a singularity is to be expected. (The seemingly artificial situation of "overlapping cylinders" ($\varepsilon < 0$), which could in principle be realized by ciliary action of micro-organisms, is considered in the Supplemental Material [8].)

In the Stokes approximation, valid at small Reynolds number, the pressure field p and velocity field $\mathbf{u} = (u, v) = (\partial\psi/\partial y, -\partial\psi/\partial x)$ satisfy the equations

$$\mu\nabla^2\mathbf{u} = \nabla p, \quad \nabla \cdot \mathbf{u} = 0, \tag{3}$$

where μ is the dynamic viscosity. The vorticity $\boldsymbol{\omega} = \nabla \times \mathbf{u} = -\nabla^2\psi \, \mathbf{e}_z$ satisfies $\nabla^2\boldsymbol{\omega} = 0$, so that ψ satisfies the biharmonic equation $\nabla^4\psi = 0$.

We shall suppose that the fluid is bounded externally by a cylinder $\mathcal{C}_0$ of radius $r = R_0 \gg 1$, on which an appropriate boundary condition can be imposed; in this way, we circumvent the problem of imposing conditions "at infinity." This is moreover needed for the numerical treatment presented in this paper, and is in any case more realistic in experimental contexts. We note the comprehensive
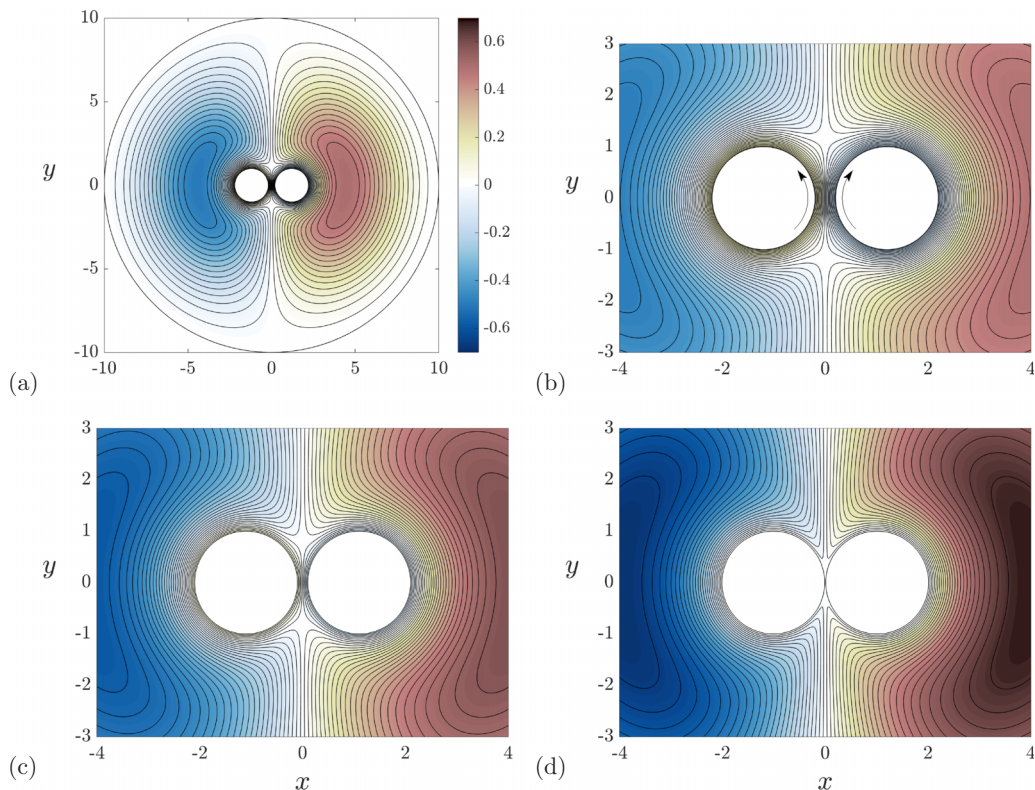
FIG. 1. Streamlines $\psi = $ const. (symmetric with respect to both x axis and y axis) from the numerical solution of the Stokes problem for counterrotating cylinders; the outer boundary condition is no-slip on $r = R_0$ (here $R_0 = 10$ and $\psi = 0$ on $r = R_0$); the color code is the same for all four panels. (a) $\varepsilon = 0.2$, full flow domain; (b) $\varepsilon = 0.2$, zoom to neighborhood of inner cylinders; the sense of rotation is indicated by the arrows; (c) same zoom for $\varepsilon = 0.1$; (d) same zoom for $\varepsilon = 0.01$. Note that the two saddle points on the y-axis approach the origin as ε decreases.

numerical and experimental investigations by Hills [9] of the 'two-roll mill' flow in a finite domain with a rectangular outer boundary. Hills used finite-difference techniques with focus on the effects of increasing Reynolds number and of change in the angular velocities of the cylinders.

The two-cylinder problem was revisited by Watson [10] who addressed Jeffery's paradox, recognizing that there may be a self-induced force per unit axial length on the pair of cylinders resulting from their counterrotation. Such a force must generate a two-dimensional stokeslet in the far flow field. Watson argued that the resulting flow should be matched asymptotically to an outer solution of the full Navier-Stokes equations, presumably a jet of the type first analyzed by Bickley [11], but this difficult matching problem remains unsolved to the present day.

The problem had been discussed earlier by Dorrepaal *et al.* [12], who showed on the basis of Jeffery's [2] solution that the force on each cylinder is zero provided Jeffery's uniform streaming at infinity is allowed for. The problem was further investigated by Elliott *et al.* [13,14] who used the boundary-element method to determine the flow for several choices of cylinder radii and angular velocities, with the conclusion that in general "the total force and the total torque (on the pair of cylinders) are both zero." This conclusion was at some variance with Watson's conclusions, published almost simultaneously.

A further approach to the two-cylinder problem was adopted by Ueda *et al.* [15], who supposed that the two cylinders are abruptly set in their rotary motion at time $t = 0$ in an initially quiescent
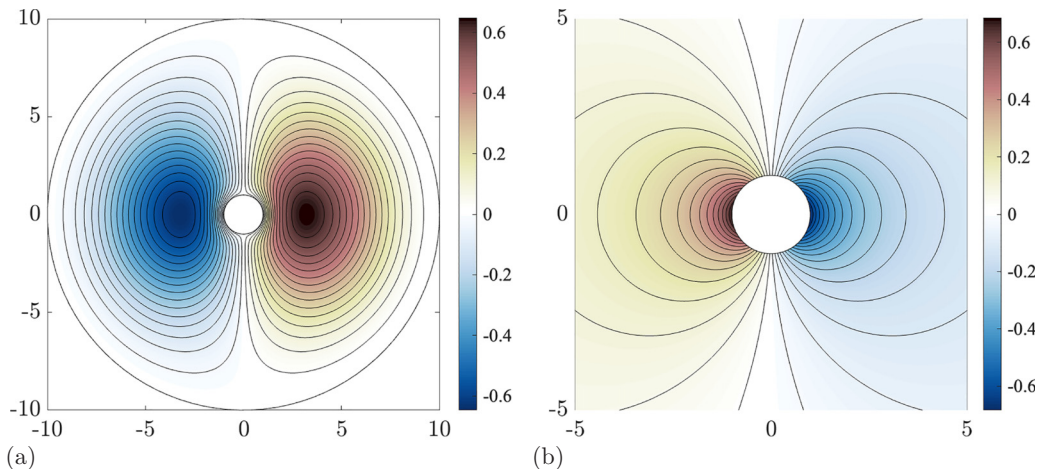
FIG. 2. Streamlines $\psi(r, \theta) = $ const. for the flow (5); (a) with no slip on $r = R_0$ (here $R_0 = 10$); (b) with no outer boundary condition ($C = D = 0$), and with $A = 0$ thus showing the instantaneous (dipole) flow in a frame fixed to the fluid at infinity.

fluid. Neglecting nonlinear inertia effects (i.e., for vanishingly small Reynolds number) and again using the boundary-element method, they studied the approach to a steady state as $t \to \infty$, and found expressions for the asymptotic force acting on each cylinder. They found a nonzero force [Fig. 6(b) of their paper] in apparent conflict with the assertion of Elliott *et al.* cited above. We note that a nonzero force implies a far-field stokeslet velocity $\sim \log r$, incompatible with the outer boundary condition imposed for all t by Ueda *et al.*, suggesting that a steady state is not attained throughout the infinite domain. The situation is indeed confusing, and calls for clarification, which we attempt to provide in the present paper.

B. A simplified model

It is helpful first to consider the following idealized problem [see Fig. 2(a)]. Suppose that fluid is contained in the annulus between two cylinders $r = 1$ and $r = R_0$, and that the boundary conditions on the inner cylinder are

$$u_r(r, \theta) \equiv r^{-1} \partial \psi / \partial \theta = 0, \quad u_\theta(r, \theta) \equiv -\partial \psi / \partial r = -\cos \theta \quad \text{on } r = 1. \tag{4}$$

Thus, we replace the two counterrotating cylinders by a single cylinder with prescribed tangential velocity on its surface—a "squirming cylinder" in the language of biofluid mechanics [16,17]. This problem has the same symmetries as the two-cylinder situation, and may be expected to give similar qualitative behavior for large R_0. Again the Reynolds number based on the boundary conditions (4) is simply $\text{Re} = \nu^{-1}$.

The general solution of $\nabla^4 \psi = 0$ proportional to $\cos \theta$ is

$$\psi(r, \theta) = (A\,r + B\,r^{-1} + C\,r \log r + D\,r^3) \cos \theta. \tag{5}$$

Here, the stokeslet term $C\,r \log r \cos \theta$ is associated with the force

$$F = -4\pi \mu C, \tag{6}$$

that the cylinder exerts on the fluid (of dynamic viscosity μ). The velocity components are

$$u_r(r, \theta) = -(A + B\,r^{-2} + C \log r + D\,r^2) \sin \theta,$$
$$u_\theta(r, \theta) = -(A - B\,r^{-2} + C(1 + \log r) + 3D\,r^2) \cos \theta, \tag{7}$$

and the boundary conditions (4) give

$$A + B + D = 0, \quad A - B + C + 3D = 1. \tag{8}$$

The no-slip conditions $u_r = u_\theta = 0$ on $r = R_0$ give the additional equations

$$A + B R_0^{-2} + C \log R_0 + D R_0^2 = 0, \quad A - B R_0^{-2} + C(1 + \log R_0) + 3D R_0^2 = 0. \tag{9}$$

Equations (8) and (9) may be solved for the constants A, B, C, D, giving

$$A = \frac{R_0^4(2 \log R_0 - 1) + 2 \log R_0 + 1}{4(R_0^2 - 1)H(R_0)}, \quad B = \frac{-\left[R_0^4(2 \log R_0 - 1) + R_0^2\right]}{4(R_0^2 - 1)H(R_0)},$$

$$C = \frac{1 - R_0^2}{2H(R_0)}, \quad D = -(A + B), \tag{10}$$

where $H(R_0) = R_0^2(\log R_0 - 1) + \log R_0 + 1$. For $\log R_0 \gg 1$, $C \sim -(2 \log R_0)^{-1}$, so from Eq. (6) the force F exerted by the cylinder on the fluid behaves like

$$F \sim 2\pi\mu / \log R_0 \quad \text{as} \quad \log R_0 \to \infty, \tag{11}$$

with very slow convergence to zero. The streamlines for this flow are shown in Fig. 2(a) for the choice $R_0 = 10$.

On $\theta = \pi/2$ and in the "inner regime" $1 \ll r \ll R_0$, the radial velocity is given asymptotically by

$$u_r(r, \pi/2) \sim -\frac{1}{2} + \frac{2 \log r - 1}{4 \log R_0} + O\left(\frac{1}{r^2 \log R_0}, \frac{r^2}{R_0^2 \log R_0}\right), \tag{12}$$

the three terms representing (in order) contributions from a uniform stream $-1/2$, the stokeslet, and a (negligible) dipole. For $1 \ll r \ll \log R_0$, the uniform stream is dominant; thus, for any fixed $r \gg 1$, the velocity tends to the uniform-stream value $-1/2$ as $\log R_0 \to \infty$.

If instead we focus on the "outer regime" where $r = O(R_0)$ as $R_0 \to \infty$, we may set $k = r/R_0$ with $\{k < 1, k = O(1)\}$; then

$$u_r(r, \pi/2) \sim \frac{k^2 - 2 \log k - 1}{4(\log R_0 - 1)} \quad \text{for } R_0 \gg 1, \quad r = O(R_0). \tag{13}$$

The ratio of inertia forces to viscous forces in this regime is given by

$$\frac{r \, u_r(r, \pi/2)}{\nu} = \frac{f(k)R_0}{\nu(\log R_0 - 1)}, \quad \text{where } f(k) = \frac{1}{4}k(k^2 - 2 \log k - 1). \tag{14}$$

The function $f(k)$ is maximal at $k \approx 0.244$, where it takes the approximate value 0.115. Hence, neglecting constants of order unity, the maximum of the expression (14) is of order $\nu^{-1}R_0 / \log R_0$ for $\log R_0 \gg 1$. This means that if

$$\frac{R_0}{\log R_0} \gtrsim \nu = \text{Re}^{-1}, \quad \text{or equivalently if} \quad R_0 \gtrsim \text{Re}^{-1} \log[\text{Re}^{-1}], \tag{15}$$

then inertia cannot be neglected in this outer regime. Thus, no matter how small Re may be, there is always an upper limit for R_0 for applicability of the Stokes approximation throughout the whole fluid domain $1 < r < R_0$.

For the same reason, in the case of an unbounded fluid domain ($R_0 = \infty$), inertia effects must intervene when

$$r \gtrsim \text{Re}^{-1} \log[\text{Re}^{-1}]. \tag{16}$$

The same limitation must surely apply to the two-cylinder problem, supporting the suggestion of Watson [10] that matching to a solution of the full Navier-Stokes equation is needed in this outer regime.
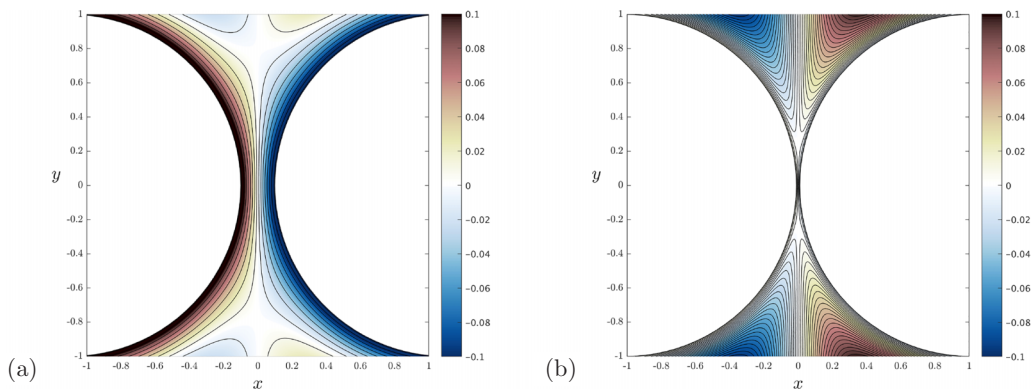
FIG. 3. As for Figs. 1(c) and 1(d), further zoomed to near the origin; (a) $\varepsilon = 0.1$; (b) $\varepsilon = 0.01$.

No outer boundary

We may note nevertheless that, if we take $C = D = 0$ in Eq. (5), thus eliminating the terms that are most divergent for large r, then we have simply $A = -B = \frac{1}{2}$, and the flow is a simple potential flow (and so an exact solution of the Navier-Stokes equation) with the uniform stream $[0, -1/2]$ at infinity. Figure 2(b) shows the instantaneous streamlines in a frame of reference fixed to the fluid at infinity; this is a dipole field. It is interesting that this "swimming flow" could be generated by ciliary action on the surface of a microscopic organism; in contrast to the conventional Stokes flow past a cylinder, the force here evaluates to zero, because the force generated by the ciliary action (4) is exactly balanced by the resulting drag force on the organism. (A similar mechanism for a spherical microscopic swimmer has been described by Lauga and Powers [17].)

C. The two-cylinder problem

1. Numerical solution

Consider now the two-cylinder counterrotating situation with nondimensionalized boundary conditions

$$\Omega_1 = 1 \text{ on } \mathcal{C}_1, \quad \Omega_2 = -1 \text{ on } \mathcal{C}_2, \quad \mathbf{u} = 0 \text{ on } \mathcal{C}_0 \, (r = R_0). \tag{17}$$

We used a finite-element procedure (details in Appendix C) to provide an accurate numerical solution. Figure 1(a) shows the streamlines $\psi = \text{const.}$ for the flow when $\varepsilon = 0.2$ and $R_0 = 10$; the arbitrary additive constant in ψ was chosen so that $\psi = 0$ on $r = R_0$. Note the presence of two saddle points near the inner cylinders on the y axis; these are more evident in the zoom of Fig. 1(b). There is an upward flux in the gap between the cylinders, and the flow due to the rotation of each cylinder exerts an upward force on the other. This joint force is transmitted to the fluid, creating a stokeslet contribution to the flow beyond the cylinders, the possibility recognized by Watson [10]; this is coupled with the downward streaming previously found by Jeffery [2] [cf Eq. (12)].

Figure 1(c) shows the same zoom when ε is reduced to 0.1. Here the saddle points have moved towards the origin, a process that is further marked in Fig. 1(d) for which $\varepsilon = 0.01$. The zoom of Fig. 3(a) to the neighborhood of the origin for the case $\varepsilon = 0.1$ makes this even more evident; Fig. 3(b) for $\varepsilon = 0.01$ shows that the saddle points are now well within the narrow gap where lubrication theory should be relevant. We shall find [see comment below Eq. (28)] that the saddle points are located at $y = \pm(6\varepsilon)^{1/2}$ as $\varepsilon \to 0$.

2. Lubrication theory

If we assume that $0 < \varepsilon \ll 1$, then lubrication theory should be applicable and reasonably accurate in the gap region. In this region, the surfaces of the two cylinders are at $x = \pm h(y)$,
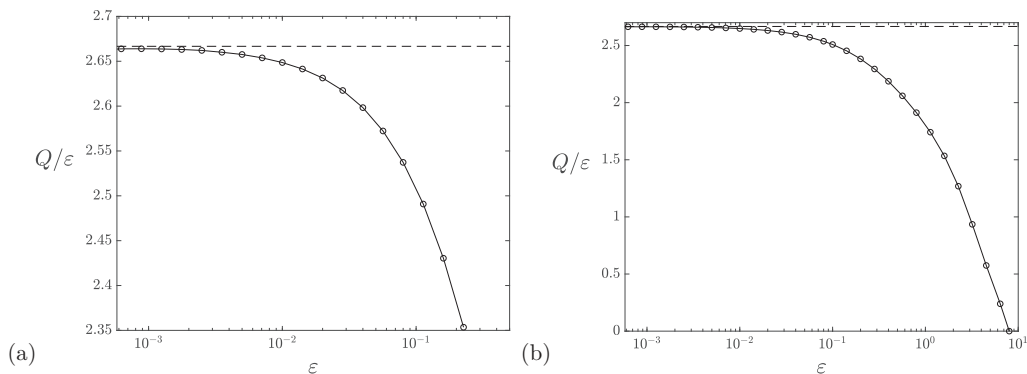
FIG. 4. (a) Normalized mass flux Q through the small gap between the cylinders as a function of ε; the dashed asymptote is at $Q/\varepsilon = 8/3 = 2.66\ldots$, as determined by lubrication theory; (b) showing that, as ε *increases* to its limiting value (8 for $R_0 = 10$, when $\mathcal{C}_1$ and $\mathcal{C}_2$ make contact with $\mathcal{C}_0$), the normalized mass flux decreases to zero.

where

$$h(y) = \varepsilon + \tfrac{1}{2}y^2 + \mathrm{O}(y^4), \quad dh/dy = y + \mathrm{O}(y^3). \tag{18}$$

We shall use a hat $\hat{\ }$ throughout to denote kinematic equivalents of dynamic quantities; thus for example pressure $p = \mu\hat{p}$, force $F = \mu\hat{F}$, etc. In the lubrication approximation ([6], Sec. 4.8), $\hat{p} = \hat{p}(y)$ and $d\hat{p}/dy = \partial^2 v/\partial x^2$, where $\mathbf{u} = (u, v)$ with $|v| \gg |u|$. This integrates with boundary conditions $v = \cos y \approx 1$ on $x = \pm h(y)$ to give

$$v(x, y) = 1 + \tfrac{1}{2}(d\hat{p}/dy)(x^2 - h(y)^2). \tag{19}$$

The flux Q between the cylinders is then

$$Q = \int_{-h(y)}^{h(y)} v(x, y)\, dx = 2\, h(y) - \frac{2}{3}\frac{d\hat{p}}{dy}\, h(y)^3, \tag{20}$$

so that

$$\frac{2}{3}\frac{d\hat{p}}{dy} = \frac{2}{h(y)^2} - \frac{Q}{h(y)^3} = \frac{2}{\left(\varepsilon + \tfrac{1}{2}y^2\right)^2} - \frac{Q}{\left(\varepsilon + \tfrac{1}{2}y^2\right)^3}. \tag{21}$$

This integrates to give the deviation of pressure from the pressure "at infinity" as

$$\hat{p}(y) = -\frac{3Qy}{2\varepsilon(y^2 + 2\varepsilon)^2} - \frac{3(3Q - 8\varepsilon)}{8\varepsilon^2}\left[\frac{y}{y^2 + 2\varepsilon} + \frac{1}{\sqrt{2\varepsilon}}\tan^{-1}[y/\sqrt{2\varepsilon}]\right]. \tag{22}$$

For large $|y|$, Eq. (22) gives

$$\hat{p}(y) \sim \pm(3\pi/16\sqrt{2})(3Q - 8\varepsilon)\varepsilon^{-5/2} + \mathrm{O}(|y|^{-3}), \tag{23}$$

and since $\hat{p}(y) \to 0$ for large $|y|$, the leading term must vanish, giving $Q = 8\,\varepsilon/3$. As expected, $Q \to 0$ as $\varepsilon \to 0$. The flux Q as a function of ε, computed from the numerical solution, is shown in Figs. 4(a) and 4(b) in which the asymptote at $Q/\varepsilon \sim 8/3 \approx 2.666$ is shown by the dashed line. The behavior here gives confidence that lubrication theory is indeed reliable when $\varepsilon \ll 1$, and that the flow in the gap is well resolved by the numerical solution for values of ε down to a few times 10^{-5}. For smaller values, numerical resolution becomes more challenging, but the lubrication description becomes increasingly accurate. With $Q = 8\varepsilon/3$, Eqs. (21) and (22) give

$$d\hat{p}/dy = [h(y)]^{-2}[3 - 4\varepsilon/h(y)], \tag{24}$$

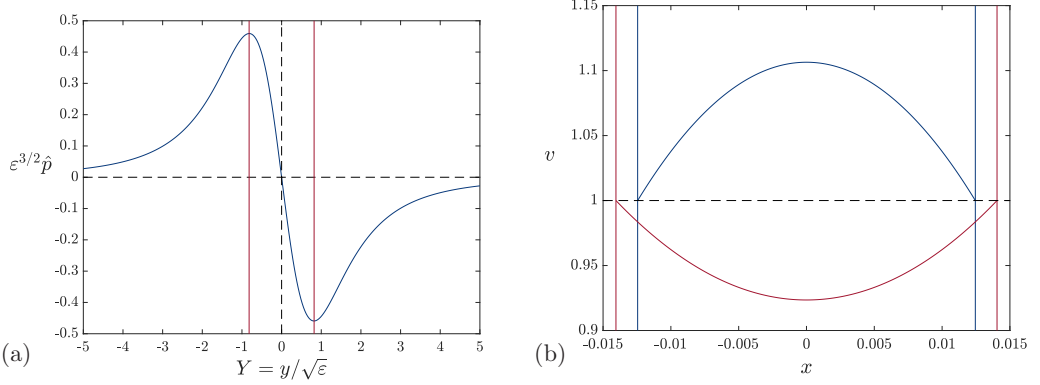FIG. 5. (a) Plot of $\varepsilon^{3/2}\hat{p}(Y)$ vs $Y = y/\sqrt{\varepsilon}$ as given by Eq. (25); (b) velocity profiles [Eq. (26)] for $\varepsilon = 10^{-2}$ at two sections, $y = 0.7\varepsilon^{1/2}$ (blue) and $y = 0.9\,\varepsilon^{1/2}$ (red); the boundaries are at $x = \pm h(y)$ in each case, and diverge as y increases; the viscous wall stress is positive for $y < 0.816\,\varepsilon^{1/2}$, negative for $y > 0.816\,\varepsilon^{1/2}$.

and, with $Y = y/\sqrt{\varepsilon}$,

$$\hat{p}(y) = -\frac{4y}{(y^2 + 2\varepsilon)^2}, \quad \text{or equivalently} \quad \varepsilon^{3/2}\,\hat{p}(Y) = -\frac{4Y}{(Y^2 + 2)^2}, \tag{25}$$

and Eq. (19) then gives

$$v(x, y) = 1 + \frac{1}{2h(y)^2}\left(3 - \frac{4\varepsilon}{h(y)}\right)(x^2 - h(y)^2). \tag{26}$$

Using the suffix L to denote the lubrication approximation, the corresponding stream function $\psi_L(x, y)$, satisfying $\partial\psi_L/\partial x = -v(x, y)$ and $\psi_L(0, y) = 0$, is

$$\psi_L(x, y) = -x - \frac{1}{2h(y)^2}\left(3 - \frac{4\varepsilon}{h(y)}\right)\left(\frac{1}{3}x^3 - h(y)^2 x\right). \tag{27}$$

The scaled pressure as a function of $Y = y/\sqrt{\varepsilon}$ is shown in Fig. 5(a). The singular behavior $p(y) \sim -4\,y^{-3}$ when $\varepsilon = 0$ is unphysical, and indicates that in practice some deformation of the cylinders must occur if they are brought into contact while rotating, a phenomenon first recognized by Hertz [18]; moreover, the liquid will cavitate where $p(y) + p_0$ falls below the vapour pressure in the region $\{y > 0, y \ll 1\}$. The singularity in pressure could presumably be resolved by taking such effects into account. This resolution problem lies outside the scope of the present treatment, and will be ignored in what follows.

The pressure gradient (24) is negative for $h(y) < 4\,\varepsilon/3$, i.e., for $|y| < (2\,\varepsilon/3)^{1/2} \approx 0.816\,\varepsilon^{1/2}$. It follows from Eq. (19) that the curvature of the velocity profile across the gap changes sign at $|y| \approx 0.816\,\varepsilon^{1/2}$. Figure 5(b) shows two velocity profiles across the gap, the blue one at $y = 0.7\,\varepsilon^{1/2}$, just below the critical level at which the curvature changes sign, the red one at $y = 0.9\,\varepsilon^{1/2}$ just above. The wall stress below the critical level $y = 0.816\,\varepsilon^{1/2}$ evidently provides a positive contribution to the force on the cylinders, while above this critical level, it provides a negative contribution. The velocity on the axis $x = 0$ is

$$v(0, y) = 1 + \frac{1}{2}\left(\frac{4\varepsilon}{h(y)} - 3\right) = \frac{2\varepsilon}{h(y)} - \frac{1}{2} = \frac{4}{2 + Y^2} - \frac{1}{2}. \tag{28}$$

This vanishes where $h(y) = 4\,\varepsilon$, i.e., at $Y = \pm\sqrt{6}$, or $y = \pm(6\varepsilon)^{1/2} \approx \pm 2.45\,\varepsilon^{1/2}$; this therefore, as previously stated, gives the location of the two saddle points on the y axis.
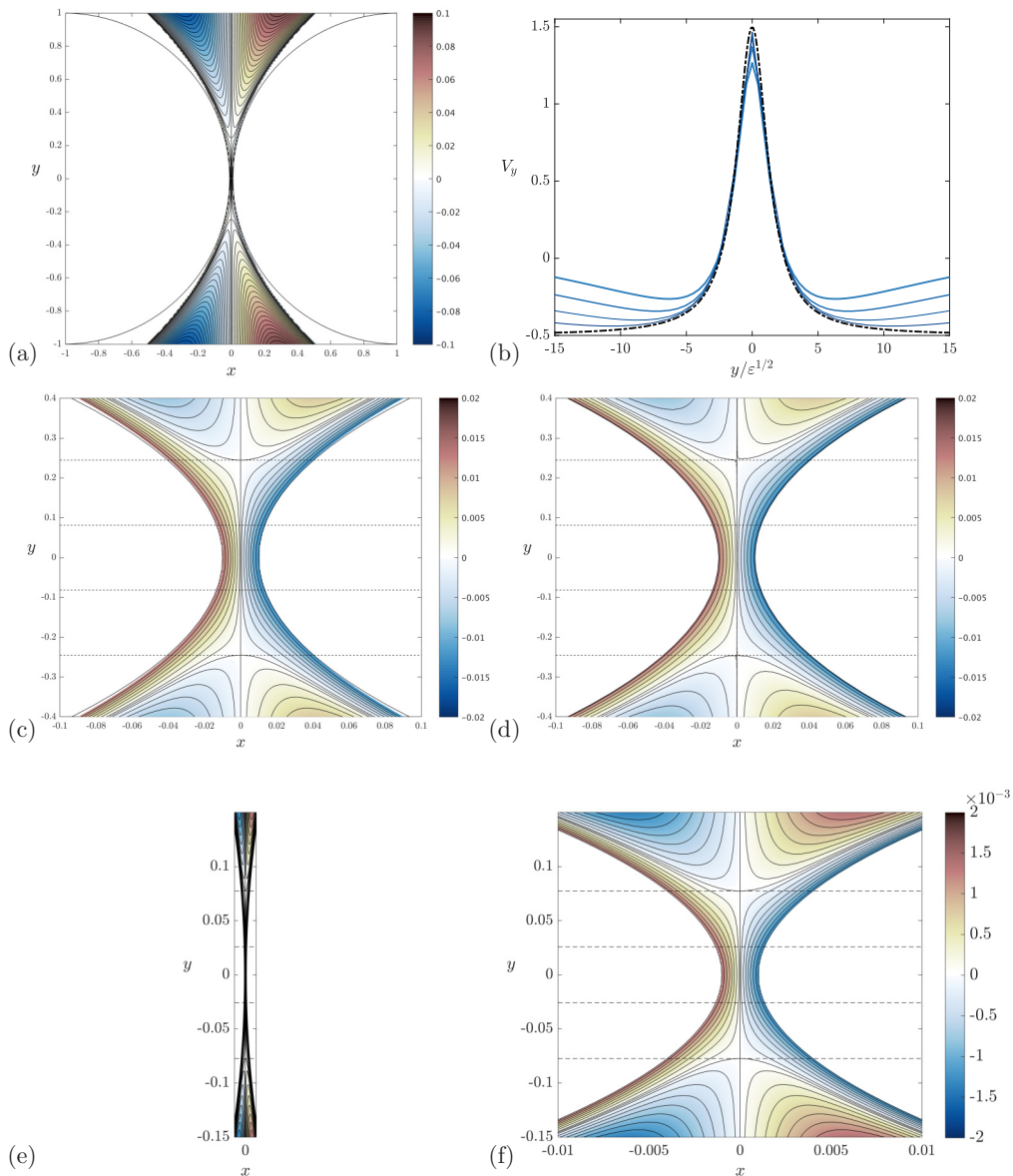
FIG. 6. (a) Streamlines $\psi_L(x, y) = $ const. as given by Eq. (27) for the case $\varepsilon = 0.01$ [compare with Fig. 3(b)]; (b) vertical velocity on the midplane $v(0, Y)$, where $Y = y/\sqrt{\varepsilon}$, for $\varepsilon = 0.2, 0.1, 0.05, 0.025$, with correspondingly decreasing line thickness; the solution determined by lubrication theory [Eq. (28)] is shown in black, dash-dotted; (c) same as panel (a), but closer to the origin and with x coordinate stretched by a factor 10; (d) the same from the full numerical solution, with the same color code; the difference is almost imperceptible. The critical levels $y = \pm 0.816\,\varepsilon^{1/2}$ and $y = \pm 2.45\,\varepsilon^{1/2}$ are shown by the dashed lines; (e) and (f) the same for the case $\varepsilon = 0.001$; (e) correct aspect ratio for this value of ε; (f) zoomed near the origin and stretched (by a factor 15) in the x direction, to show more details of the structure; the critical levels $y = \pm 0.816\,\varepsilon^{1/2}$ and $y = \pm 2.45\,\varepsilon^{1/2}$ are again shown by the dashed lines.
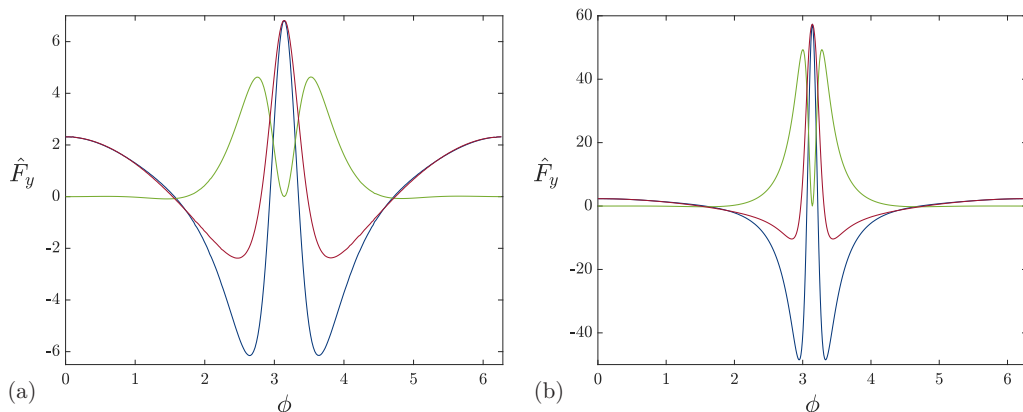
FIG. 7. Distribution of the vertical forces on $\mathcal{C}_2$ as functions of the angle ϕ; the narrowest point of the gap is at $\phi = \pi$; $R_0 = 10$; viscous term (blue), pressure term (green), total force (red); (a) $\varepsilon = 10^{-1}$; (b) $\varepsilon = 10^{-2}$.

Figure 6(a) shows the streamlines $\psi_L =$ const. given by Eq. (27) for $\varepsilon = 0.01$, which admits comparison with the numerical solution shown in Fig. 3(b). Figure 6(c) shows the same nearer the origin with the x coordinate stretched by a factor 10, and Fig. 6(d) shows the same streamlines as determined by the full numerical solution; the difference here is almost imperceptible, again giving confidence in the accuracy of both the numerics and the lubrication theory at least at this value of $\varepsilon = 0.01$. In both panels, the critical levels $y = \pm 0.816 \, \varepsilon^{1/2}$ (at which the viscous wall stress changes sign) and $y = \pm 2.45 \, \varepsilon^{1/2}$ (at which the saddle points occur) are shown by the dashed lines.

Figure 6(b) shows the vertical velocity on the midplane $v(0, Y)$, where $Y = y/\sqrt{\varepsilon}$, for $\varepsilon = 0.2, 0.1, 0.05, 0.025$, with correspondingly decreasing line thickness, and the limiting curve (dash-dotted) as given by lubrication theory [Eq. (28)]. The curves shadow the limiting curve ever more faithfully as ε decreases, giving further confidence in the relevance of the limiting lubrication-theory treatment.

Figure 6(e) shows the streamlines in the gap as given by Eq. (27) for the even smaller value $\varepsilon = 0.001$, and Fig. 6(f) shows the same zoomed near the origin and stretched in the x direction, again revealing the saddle-point structure.

3. Force on the cylinders, as determined by lubrication theory

The vertical force μF_y on each cylinder consists of two parts: (i) the shear stress (viscous) force $F_{yv} = \mu \hat{F}_{yv}$ and (ii) the pressure force $F_{yp} = \mu \hat{F}_{yp}$; for $\varepsilon > 0$, these are given by

$$\hat{F}_{yv} = -\int_{-\infty}^{\infty} \frac{\partial v}{\partial x}\bigg|_{x=h(y)} dy = \int_{-\infty}^{\infty} \frac{4\varepsilon - 6y^2}{(y^2 + 2\varepsilon)^2} \, dy = -\pi (2/\varepsilon)^{1/2}, \tag{29}$$

and

$$\hat{F}_{yp} = \int_{-\infty}^{\infty} \hat{p}\left(-\frac{dh}{dy}\right) dy = \int_{-\infty}^{\infty} \frac{4y^2}{(y^2 + 2\varepsilon)^2} \, dy = \pi (2/\varepsilon)^{1/2}, \tag{30}$$

so that

$$\hat{F}_{yv} + \hat{F}_{yp} = \int_{-\infty}^{\infty} \frac{4\varepsilon - 2y^2}{(y^2 + 2\varepsilon)^2} \, dy = 0. \tag{31}$$

Thus, somewhat surprisingly, the total force on each cylinder vanishes at $\mathrm{O}(\varepsilon^{-1/2})$. This conclusion is however supported by the numerical solution: Fig. 7 shows the distribution of the two contributions to the vertical force as functions of the angle ϕ round $\mathcal{C}_2$, confirming that the forces are
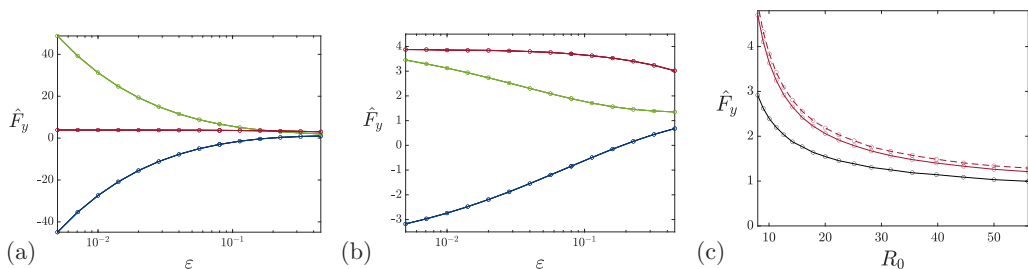
FIG. 8. (a) Integrated contributions to the vertical force on $\mathcal{C}_2$, viscous (blue), pressure (green) and the total (red), as functions of ε; (b) the same, but with the viscous and pressure contributions rescaled by $\sqrt{\varepsilon}$ (the total force is not rescaled); (c) dependence of total force on R_0, $\varepsilon = 0.1$ (solid), $\varepsilon = 0.01$ (dashed); no-slip condition on $\mathcal{C}_0$ (red), stress-free condition on $\mathcal{C}_0$ (black).

indeed increasingly concentrated near the minimum gap position $\phi = \pi$ as ε decreases; and Fig. 8 shows that when $R_0 = 10$ the integrated pressure and viscous contributions do indeed nearly cancel at O($\varepsilon^{-1/2}$), but that there is an O(1) residual contribution $\hat{F}_{yv} + \hat{F}_{yp} \approx 3.9$ for $0 < \varepsilon \ll 1$, a result that lies outside the scope of the leading-order lubrication approximation. We might expect that this residual force should decrease to zero as R_0 increases without limit, in conformity with Jeffery's [2] conclusion; Fig. 8(c) shows that the force does decrease at least in the range $8 < R_0 < 55$; this dependence implies that the force, being dependent on the far-field, cannot be obtained even by the higher-order, but still local, lubrication theory of Tavakol *et al.* [19]. From comparison with the model problem of Part I B above, it is almost certain that $\hat{F}_y \sim (\log R_0)^{-1}$ as R_0 increases, i.e., extremely slowly. When $R_0 \to \infty$ at fixed Reynolds number Re $\ll 1$, inertia effects in the far field require that we replace R_0 by $r \sim \mathrm{Re}^{-1} \log [\mathrm{Re}^{-1}]$ [see Eq. (16) above]; it thus seems likely that the decrease of $\hat{F}_y$ will satisfy

$$\hat{F}_y \sim (\log[\mathrm{Re}^{-1} \log [\mathrm{Re}^{-1}]])^{-1} \quad \text{when } R_0 \gg \mathrm{Re}^{-1} \gg 1, \tag{32}$$

although proof of this would require matching to an appropriate far-field solution.

But what if $\varepsilon = 0$? In this situation, when the cylinders make contact, the integrand in Eq. (31) is $-2/y^2$, and the integral diverges. The force $\hat{F}_{yv} + \hat{F}_{yp}$ is then apparently infinite! The situation can be understood with reference to Fig. 9, which shows a plot of the integrand in Eq. (31) for $\varepsilon = 10^{-5}$ (blue), 5×10^{-6} (green), and $\varepsilon = 0$ (red). As ε decreases the curves approach the limit curve more and more closely. The spike in the region $|y| < (2\varepsilon)^{1/2}$ contributes the positive value to the integral that exactly compensates the negative value from the region $|y| > (2\varepsilon)^{1/2}$. When $\varepsilon = 0$, the spike disappears, and only the negative contribution survives.

However, in this limit situation when the cylinders make contact, there is a pressure discontinuity across the point of contact, and this can contribute a force $\hat{F}_c$ to the resultant total force on the two cylinders. We describe this as a 'flow-induced contact force', because it arises as a *net* force *on the pair of cylinders* due to the contact between them in the presence of flow. [This must be distinguished from the more familiar (equal and opposite) "solid contact force" that may be experienced by *each* cylinder by virtue of their contact.] This flow-induced contact force can be obtained as follows.

4. Flow-induced contact force

We need simply consider the restricted domain of fluid inside the blue contour shown in Fig. 9(b) for the contact situation $\varepsilon = 0$ with $h(y) = \frac{1}{2}y^2$. The short segment in this figure is at the level $y = y_1$. The total force on the curved parts of the blue contour is

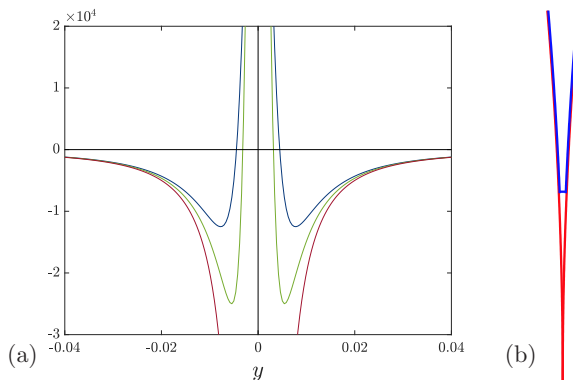$$2 \int_{y_1}^{\infty} \frac{(-2y^2)}{y^4} \, dy = -4/y_1. \tag{33}$$

FIG. 9. (a) Plot of the function $(4\varepsilon - 2y^2)/(y^2 + 2\varepsilon)^2$, for $\varepsilon = 10^{-5}$ (blue), 5×10^{-6} (green), and $\varepsilon = 0$ (red). As $\varepsilon \downarrow 0$, the spike at $y = 0$ becomes longer and narrower, and ultimately disappears in the limit $\varepsilon = 0$; (b) contour (shown in blue) used for calculation of the contact force when $\varepsilon = 0$; the short segment is at the level $y = y_1$, and the limit $y_1 \downarrow 0$ is considered.

From Eq. (25), when $\varepsilon = 0$, the pressure is given by $\hat{p} = -4/y^3$, so the pressure force on the small horizontal segment (an upwards suction) is

$$\int_{-h(y_1)}^{h(y_1)} -\hat{p}\,dx = (4/y_1^3)y_1^2 = +4/y_1. \tag{34}$$

This exactly balances the force (33) from the curved parts of the contour. (These forces are $\pm 8/y_1$ when contributions from the region $y < 0$ are also taken into account.) This force balance persists in the limit $y_1 \downarrow 0$, and we may conclude that what was the upward contribution to $\hat{F}_{yv} + \hat{F}_{yp}$ when $\varepsilon > 0$ is replaced when $\varepsilon = 0$ by the upward contact force resulting from the (infinite) jump in pressure across the point of contact. (This argument ignores cavitation, which must break the symmetry of the limiting flow across $y = 0$.)

The analytic treatment of this limit that now follows provides an alternative derivation of this contact force that does not rely on the lubrication approximation.

D. Analytic solution when $\varepsilon = 0$ and $R_0 = \infty$

When $\varepsilon = 0$ and $R_0 = \infty$, the Stokes problem may be solved exactly; this is the limit version of Jeffery's [2] problem (see Appendix A). Following Schubert [20], we use the conformal mapping $\zeta \equiv \xi + i\eta = 1/z$, where $z \equiv x + iy$, giving

$$\xi = \frac{x}{x^2 + y^2}, \quad \eta = \frac{-y}{x^2 + y^2}. \tag{35}$$

The scale factor for this mapping is

$$h(\xi, \eta) = |d\zeta/dz| = (x^2 + y^2)^{-1} = \xi^2 + \eta^2. \tag{36}$$

The contours $\xi = \text{const.}$, $\eta = \text{const.}$, are the circles shown in Fig. 10(a). The essential property of this mapping is that $\psi(x, y)$ satisfies the biharmonic equation $\nabla^4 \psi = 0$ if and only if $\Psi(\xi, \eta) = h(\xi, \eta)\psi[x(\xi, \eta), y(\xi, \eta)]$ satisfies $\nabla^4_{\xi,\eta}\Psi = 0$.

For our problem, we want a solution of $\nabla^4 \psi = 0$ that is antisymmetric about $x = 0$, or equivalently a solution of $\nabla^4_{\xi,\eta}\Psi = 0$ antisymmetric about $\xi = 0$. We also need to impose angular velocities ± 1 on the circles $\xi = \mp 1/2$. The boundary conditions are then

$$\Psi = \Psi_{\xi\xi} = 0 \quad \text{on} \quad \xi = 0, \quad \text{and} \quad \Psi = 0, \ \Psi_\xi = -1 \quad \text{on} \quad \xi = \pm 1/2. \tag{37}$$

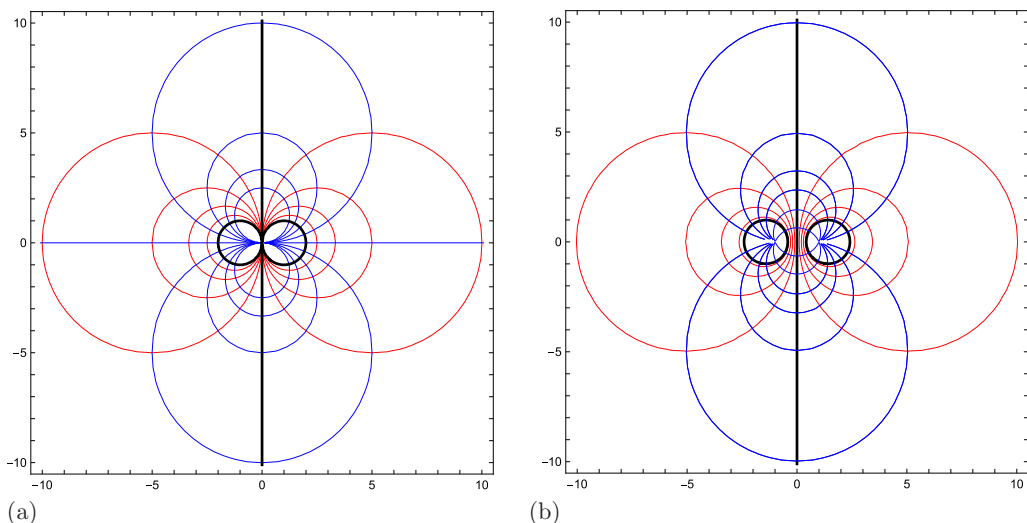FIG. 10. (a) Contours $\xi = $ const. (red) and $\eta = $ const. (blue), given by Eq. (35); the contours $\xi = 0, \pm 1/2$ are shown in black; (b) corresponding contours given by the conformal mapping $\zeta = \log[(z + c)/(z - c)]$, as used by Jeffery [2] here $c = 1$ and the cylinders of unit radius are shown by the contours $\xi = \pm \sinh^{-1} c \approx \pm 0.881$.

The required solution evidently does not depend on η; it is given by $\Psi(\xi, \eta) = \xi/2 - 2\xi^3$, and correspondingly

$$\psi(x, y) = (x^2 + y^2)\Psi(\xi, \eta) = x/2 - 2x^3(x^2 + y^2)^{-2} = x/2 - \frac{\partial}{\partial x}\left[\frac{y^2}{x^2 + y^2} + \log(x^2 + y^2)\right]. \tag{38}$$

In plane polar coordinates $\{r, \theta\}$, this is equivalently

$$\psi(r, \theta) = \tfrac{1}{2}r\cos\theta - \tfrac{1}{2}r^{-1}(3\cos\theta + \cos 3\theta), \tag{39}$$

which does indeed satisfy $\nabla^4\psi = 0$. The streamlines $\psi = $ const. are shown in Fig. 11(a), and a zoom near the point of contact in Fig. 11(b). The leading term $x/2$ in Eq. (38) represents the Jeffery uniform stream [$(0, -\tfrac{1}{2})$ in this contact limit], while the term $-2x^3(x^2 + y^2)^{-2}$ admits interpretation as the flow due to a "torque doublet" (or, to coin a suitable word comparable to stresslet [21], a
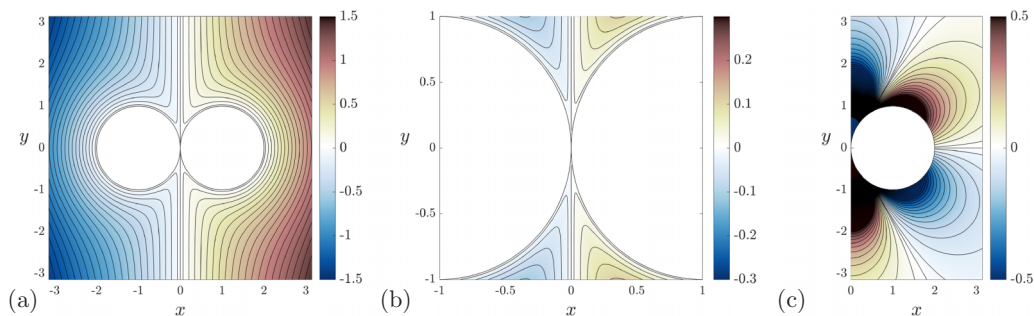

FIG. 11. (a) Streamlines $\psi = $ const., as given by Eq. (38); (b) zoom near the point of contact; (c) contours $\hat{p} = $ const. in the half-plane $x > 0$ as given by Eq. (43).
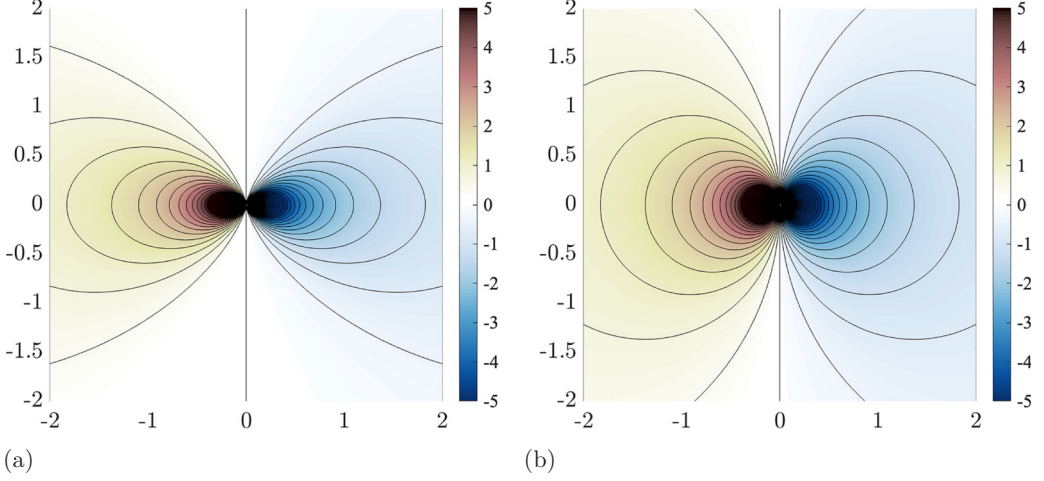
FIG. 12. (a) Streamlines associated with the torquelet $\psi_T = -(\partial/\partial x)(\log r^2 + \sin^2 \theta)$; (b) streamlines associated with the vortex dipole $\psi_V = -(\partial/\partial x)(\log r^2)$. The torquelet streamlines appear to be more compressed towards the plane $y = 0$.

"torquelet"):

$$\psi_T = -(\partial/\partial x)(\log r^2 + \sin^2 \theta). \tag{40}$$

The streamlines of the torquelet $\psi_T =$ cst. are shown in Fig. 12(a); the apparent compression of the streamlines towards the plane $y = 0$ as compared with the streamlines of the simpler vortex dipole $\psi_V = -(\partial/\partial x)(\log r^2)$ [Eq. (12)] is evident. This compression is due to the no-slip condition on the two rotating cylinders and their resulting mutual influence, an effect that evidently persists to the far field in the fluid.

1. Pressure field

The velocity components are

$$u(x, y) = \frac{\partial \psi}{\partial y} = \frac{8x^3 y}{(x^2 + y^2)^3}, \quad v(x, y) = -\frac{\partial \psi}{\partial x} = -\frac{1}{2} - \frac{2(x^4 - 3x^2 y^2)}{(x^2 + y^2)^3}, \tag{41}$$

and the pressure field satisfies the equations

$$\frac{\partial \hat{p}}{\partial x} = \nabla^2 u = -\frac{48xy(x^2 - y^2)}{(x^2 + y^2)^4}, \quad \frac{\partial \hat{p}}{\partial y} = \nabla^2 v = \frac{12(x^4 - 6x^2 y^2 + y^4)}{(x^2 + y^2)^4}. \tag{42}$$

Either of these equations may be integrated, giving

$$\hat{p}(x, y) = 4y(3x^2 - y^2)(x^2 + y^2)^{-3}. \tag{43}$$

The contours $\hat{p}(x, y) =$ const. in the half-plane $x \geqslant 0$ are shown in Fig. 11(c).

On the right-hand cylinder $\mathcal{C}_2$, let

$$x = 1 + \cos \phi, \quad y = \sin \phi, \quad (-\pi \leqslant \phi \leqslant \pi), \quad \text{so} \quad r^2 \equiv x^2 + y^2 = 2(1 + \cos \phi). \tag{44}$$

The normal and tangent vectors on $\mathcal{C}_2$ have cartesian components

$$\mathbf{n} = (\cos \phi, \sin \phi), \quad \mathbf{t} = (-\sin \phi, \cos \phi). \tag{45}$$

From Eq. (43), the pressure on $\mathcal{C}_2$ is then

$$\hat{p}(\phi) = \tfrac{1}{2} \sin \phi [3(1 + \cos \phi)^2 - \sin^2 \phi](1 + \cos \phi)^{-3}. \tag{46}$$

The vertical component of the pressure force $-\hat{p}\,\mathbf{n}$ on $\mathcal{C}_2$ is $-\hat{p}(\phi)\sin\phi$, which has the asymptotic behavior

$$-\hat{p}(\phi)\sin\phi \sim 4(\phi - \pi)^{-2} \quad \text{near} \quad \phi = \pi, \tag{47}$$

obviously nonintegrable at the point of contact $\phi = \pi$.

2. Viscous stress on cylinder

The rate-of strain components are

$$e_{11} = \partial u/\partial x, \quad e_{12} = e_{21} = \tfrac{1}{2}(\partial u/\partial y + \partial v/\partial x), \quad e_{22} = \partial v/\partial y. \tag{48}$$

Substituting Eq. (41), and simplifying leads to the results

$$e_{11}(x, y) = -e_{22}(x, y) = \frac{24y(x^2 y^2 - x^4)}{(x^2 + y^2)^4}, \quad e_{12}(x, y) = \frac{6x(x^4 - 6x^2 y^2 + y^4)}{(x^2 + y^2)^4}. \tag{49}$$

On the cylinder $\mathcal{C}_2$ with parametric equations (44), these reduce to

$$e_{11}(\phi) = -e_{22}(\phi) = \frac{-3\sin 2\phi}{2(1 + \cos\phi)}, \quad e_{12}(\phi) = \frac{3\cos 2\phi}{2(1 + \cos\phi)}. \tag{50}$$

The viscous stress components $\tau_1(\phi) = \mu\,\hat{\tau}_1(\phi)$ and $\tau_2(\phi) = \mu\,\hat{\tau}_2(\phi)$ on $\mathcal{C}_2$ are given by

$$\hat{\tau}_1(\phi) = 2(e_{11}(\phi)\cos\phi + e_{12}(\phi)\sin\phi), \quad \hat{\tau}_2(\phi) = 2(e_{21}(\phi)\cos\phi + e_{22}(\phi)\sin\phi), \tag{51}$$

and these reduce to

$$\hat{\tau}_1(\phi) = -3\sin\phi(1 + \cos\phi)^{-1}, \quad \hat{\tau}_2(\phi) = 3\cos\phi(1 + \cos\phi)^{-1}, \tag{52}$$

with the asymptotic behavior near $\phi = \pi$,

$$\hat{\tau}_1(\phi) \sim 6(\pi - \phi)^{-1}, \quad \hat{\tau}_2(\phi) \sim -6(\pi - \phi)^{-2}. \tag{53}$$

Note that the total vertical component of stress on $\mathcal{C}_2$, $-\hat{p}(\phi)\sin\phi + \hat{\tau}_2(\phi)$, therefore behaves like $-2(\pi - \phi)^{-2}$ near $\phi - \pi$, and is therefore nonintegrable, indicating an infinite integrated downward contribution to the vertical force.

3. Confirmation of flow-induced contact force

To resolve this singularity, we consider the vertical force now integrated round the closed contour shown in red in Fig. 13, as described in the figure caption. The integral of the vertical force component round $\mathcal{C}_2$ from $\phi = -\phi_1$ to $\phi = \phi_1$ is, with some simplification,

$$\int_{-\phi_1}^{\phi_1} (-\hat{p}(\phi)\sin\phi + \hat{\tau}_2(\phi))\,d\phi = \int_{-\phi_1}^{\phi_1} \frac{2\cos\phi + \cos 2\phi}{1 + \cos\phi}\,d\phi = 2\sin(3\phi_1/2)\sec(\phi_1/2). \tag{54}$$

The contribution to $\hat{F}_{yp} + \hat{F}_{yv}$ from both $\mathcal{C}_1$ and $\mathcal{C}_2$ is therefore

$$4\sin(3\phi_1/2)\sec(\phi_1/2) \sim -8(\pi - \phi_1)^{-1} + \tfrac{26}{3}(\pi - \phi_1) + \mathrm{O}(\pi - \phi_1)^3, \tag{55}$$

which is indeed singular as $\phi_1 \to \pi$. However, as in Part I C 2, there is also a contribution to the total vertical force from the small segments at $y = \pm y_1$; this is

$$\hat{F}_c = \int_{-h(y_1)}^{h(y_1)} [\hat{p}(x, -y_1) - \hat{p}(x, y_1)]\,dx = \frac{128}{y_1(4 + y_1)^2} \sim \frac{8}{y_1} - 4y_1 + \mathrm{O}(y_1^3), \tag{56}$$

and, since $y_1 \sim \pi - \phi_1$, the singularity here exactly cancels the singularity in Eq. (55) as $y_1 \to 0$. Moreover since this leaves terms of order y_1 which vanish in the limit, it follows that, in the limit, the total net force on the composite body is zero:

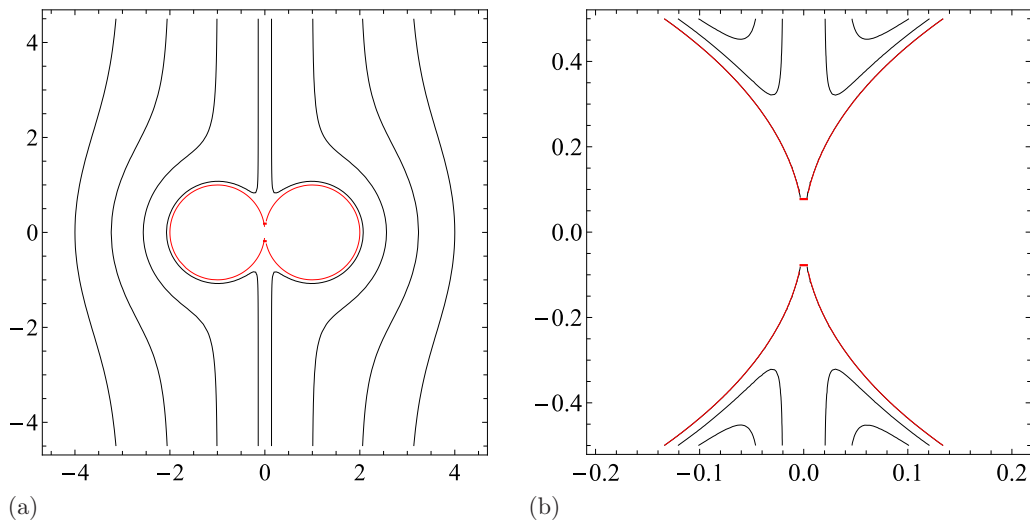$$\hat{F}_y = \lim_{y_1 \to 0} (\hat{F}_{yp} + \hat{F}_{yv} + \hat{F}_c) = 0. \tag{57}$$

FIG. 13. (a) Contour of integration (shown in red) for calculating the total resultant vertical force on both cylinders when they make contact ($\varepsilon = 0$); the integral round the right-hand cylinder $\mathcal{C}_2$ runs from $\phi = -\phi_1$ to $\phi = \phi_1$, where $0 < \pi - \phi_1 \ll 1$ (and this is equal, by symmetry, to the contribution from $\mathcal{C}_1$); and the integral on the small horizontal segments at $y = \pm y_1$ run from $x = -y_1^2/2$ to $y_1^2/2$, where $y_1 = \sin\phi_1 = \sin(\pi - \phi_1) \sim \pi - \phi_1$; we then take the limit $\phi_1 \to \pi$ (i.e., $y_1 \to 0$); (b) zoom near the origin, and expanded by a factor of 2 in the x direction to make the short sections at $y = \pm y_1$ more clearly visible.

This is consistent with the result (31), implying that the conclusion that the force is zero is in fact valid for all $\varepsilon \geqslant 0$. This also confirms the validity of the previous simpler derivation of the same force balance under the lubrication approximation. We shall see in Part I E below how $\frac{1}{2}\hat{F}_c$ exerts part of the torque that each cylinder experiences about its axis.

Note that in a frame of reference fixed in the fluid at infinity, the two cylinders move with velocity $\mathbf{V} = (0, \frac{1}{2})$. The force generated by their rotation is then equal and opposite to the drag force that they jointly experience as they move through the fluid; in effect the velocity $\mathbf{V}$ is just such that this force balance is exactly satisfied.

E. Torque on the cylinders

1. Torque when $\varepsilon > 0$

Since the total force on each cylinder, including the contact force, is zero (when $R_0 \to \infty$), the torques $\hat{\mathcal{T}}_1 \mathbf{e}_z$ and $\hat{\mathcal{T}}_2 \mathbf{e}_z = \hat{\mathcal{T}}_1 \mathbf{e}_z$ acting on $\mathcal{C}_{1,2}$ are independent of the point relative to which the torque is calculated, e.g., $\hat{\mathcal{T}}_2$ is the same whether calculated relative to the center of $\mathcal{C}_2$ or relative to the origin O. When $0 < \varepsilon \ll 1$, the viscous drag on $\mathcal{C}_2$ is concentrated near the gap point $(\varepsilon, 0)$ and the pressure on $\mathcal{C}_2$ makes no contribution to the torque about its axis at $(1 + \varepsilon, 0)$; hence, using Eq. (29), this torque is given by

$$\hat{\mathcal{T}}_2 \sim -\hat{F}_{yv} \sim \pi(2/\varepsilon)^{1/2}. \tag{58}$$

Figure 14(a) shows the torque $\hat{\mathcal{T}}_2(\alpha)$ (where $\alpha \sim (2\varepsilon)^{1/2}$) computed both from our numerical solution for $R_0 = 10$ (blue) and 15 (red), and from Jeffery's solution [2] as described in Appendix A (black), and Fig. 14(b) shows the corresponding compensated functions $\alpha \hat{\mathcal{T}}_2(\alpha)$. The convergence as R_0 increases is evident, and it is clear that, in the limit $R_0 \to \infty$, $\hat{\mathcal{T}}_2(\alpha) \sim 2\pi/\alpha$ as $\alpha \to 0$, in perfect agreement with the asymptotic result (58).

The pair of torques $\pm\hat{\mathcal{T}}_2(\alpha)$ do indeed constitute a torquelet associated with the term $-\frac{1}{2}r^{-1}(3\cos\theta + \cos 3\theta)$ in Eq. (39). We shall confirm in Appendix A that Eq. (39) is the limit as
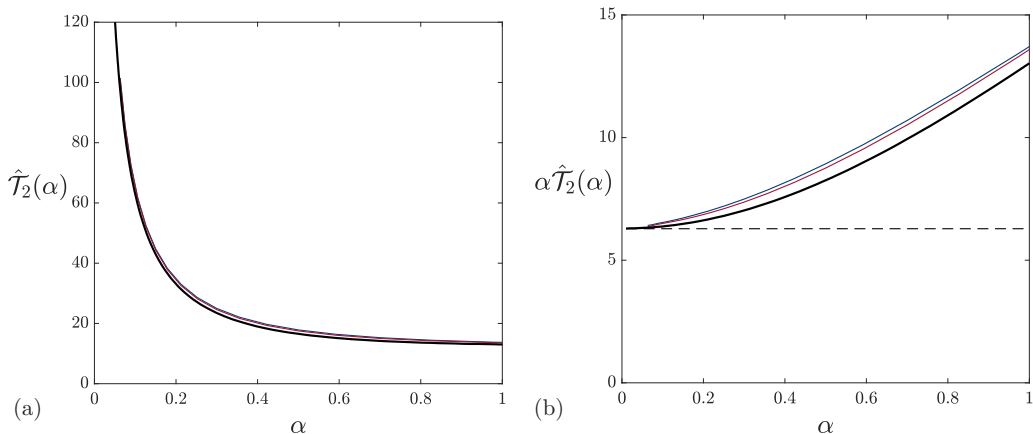
FIG. 14. (a) The torque $\hat{\mathcal{T}}_2(\alpha)$ where $\alpha = \cosh^{-1}(1 + \varepsilon) \sim (2\varepsilon)^{1/2}$, computed from Jeffery's solution (see Appendix A, in black), and from the full numerics with $R_0 = 10$ (in blue), and $R_0 = 15$ (in red); (b) The function $\alpha\hat{\mathcal{T}}_2(\alpha)$ with the same color code; the level 2π is shown by the dashed line, showing that $\hat{\mathcal{T}}_2(\alpha) \sim 2\pi/\alpha = \pi(2/\varepsilon)^{1/2}$ as $\alpha \to 0$.

$\varepsilon \to 0$ of the solution found by Jeffery [2] and that the torquelet ingredient of this flow is associated in the limit $\alpha \sim (2\varepsilon)^{1/2} \to 0$ with torque singularities $\pm\hat{\mathcal{T}}_2(\alpha) \sim \pm 2\pi/\alpha$ separated by the vanishing distance $d(\alpha) \sim 3\alpha$.

2. Torque when $\varepsilon = 0$

When $\varepsilon = 0$, it is instructive also to calculate the asymptotic behavior of this torque as a function of the cut-off level y_1 defined in Fig. 13. From the cartesian stress components (52), the tangential stress on $\mathcal{C}_2$ is

$$\hat{\tau}(\phi) = \hat{\tau}_2(\phi)\cos\phi - \hat{\tau}_1(\phi)\sin\phi = 3(1 + \cos\phi)^{-1}. \tag{59}$$

Integrating this from $-\phi_1$ to $+\phi_1$ where $\pi - \phi_1 \sim y_1 \ll 1$ gives the moment of this tangential stress as

$$\hat{M}_v = \int_{-\phi_1}^{\phi_1} \frac{3}{1 + \cos\phi}\, d\phi = 6\tan(\phi_1/2) \sim \frac{12}{\pi - \phi_1} \quad \text{as } \phi_1 \to \pi. \tag{60}$$

There is also a contribution from the moment of the half of the contact force $\hat{F}_c$ that can be deemed to act on $\mathcal{C}_2$, viz., $\hat{M}_c = -\frac{1}{2}\hat{F}_c \sim -4/y_1$ from Eq. (56). Combining these moments gives the torque

$$\hat{\mathcal{T}}_2(y_1) = \hat{M}_v + \hat{M}_c \sim 8/y_1 \quad \text{as } y_1 \to 0, \tag{61}$$

and we note again that, by symmetry, $\hat{\mathcal{T}}_1(y_1) = -\hat{\mathcal{T}}_2(y_1)$.

Alternatively, we may calculate this same torque relative to the origin O. The tangential stress $\hat{\tau}(\phi)$ exerts a moment $(\mathbf{x} \times \mathbf{t})\hat{\tau}(\phi)$ about the contact point O(0, 0); here,

$$\mathbf{x} = (1 + \cos\phi, \sin\phi) \quad \text{and} \quad \mathbf{t} = (-\sin\phi, \cos\phi), \quad \text{so} \quad \mathbf{x} \times \mathbf{t} = (1 + \cos\phi)\mathbf{e}_z, \tag{62}$$

and it follows remarkably that this moment takes the value 3, uniform on $\mathcal{C}_2$, so that the total moment of the tangential stress about O takes the finite value $\hat{M}_{Ov} = 3(2\pi) = 6\pi$. However, noting that

$$\mathbf{x} \times \mathbf{n} = (1 + \cos\phi, \sin\phi) \times (\cos\phi, \sin\phi) = \sin\phi\, \mathbf{e}_z \quad \text{on } \mathcal{C}_2, \tag{63}$$
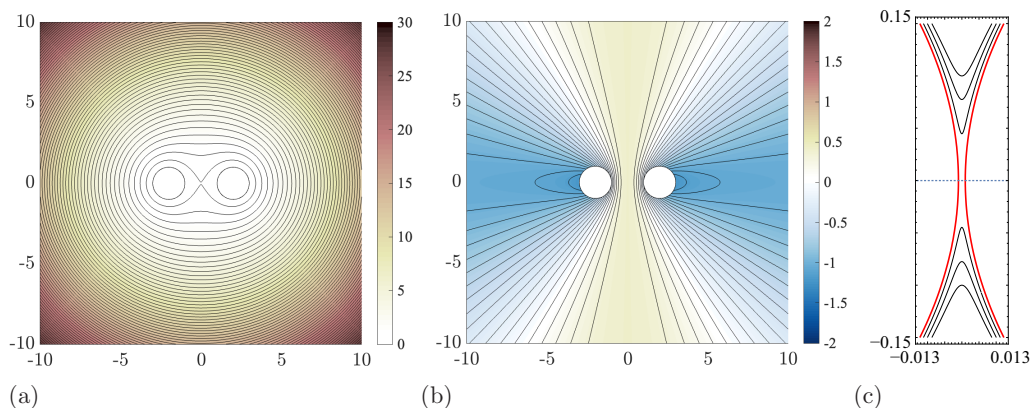
FIG. 15. (a) Streamlines $\psi_{J2}(x, y, \alpha) = $ const. as given by Eq. (69), for the choice $\epsilon = 1$ ($\alpha = 1.317$); the flow asymptotes rapidly to rigid body rotation $\Omega(\alpha) = -0.275$; (b) streamlines in rotating frame, exhibiting the radial flow in the far field with $\Lambda(\alpha) = -1.449$; (c) contours $\psi_L(x, y) = $ const. in the narrow gap, for corotating cylinders with $\varepsilon = 0.001$.

it is actually the pressure $-\hat{p}(\phi)\mathbf{n}$ on $\mathcal{C}_2$ that exerts the dominant moment about O; using Eqs. (46) and (63), this is

$$\hat{M}_{Op} = \int_{-\phi_1}^{\phi_1} -\hat{p}(\phi)\sin\phi\, d\phi = -6\phi + 4\sin\phi + 4\tan(\phi/2) \sim \frac{8}{\pi - \phi_1} - 6\pi, \qquad (64)$$

and so the torque relative to O is

$$\hat{\mathcal{T}}_2(y_1) = \hat{M}_{Ov} + \hat{M}_{Op} \sim 8/y_1 \quad \text{as } y_1 \sim \pi - \phi_1 \to 0, \qquad (65)$$

in precise agreement with Eq. (61). We should note here that the flow-induced contact force has zero moment about O in the limit $y_1 \to 0$.

PART II: COROTATING CYLINDERS

A. An elementary model problem

Figure 15(a) shows the symmetries of the flow induced by corotating cylinders. We recall first an elementary model problem that exhibits the same symmetries as those of this figure, namely the problem of flow in an annulus $1 < r < R_0$, $R_0 \gg 1$, when the inner cylinder $r = 1$ rotates with angular velocity $\Omega = -1$, and the outer cylinder $r = R_0$ is at rest. The flow in the annulus is purely azimuthal,

$$\mathbf{u} = [0, v(r)] \quad \text{where } v(r) = Ar + B/r \quad \text{with } A + B = -1. \qquad (66)$$

There are two quite distinct possible scenarios:

(i) We may impose a "zero-stress" condition, $d(v/r)/dr = 0$, on $r = R_0$; then $B = 0$ and $v(r) = -r$, rigid-body rotation throughout the fluid, obviously nonzero at infinity when $R_0 \to \infty$. The torque acting on the cylinder is zero in this situation. This is the scenario that is apparent in Jeffery's [2] approach to the two-cylinder problem described in Part II C 1 and Part II C 2 below.

(ii) Alternatively, we may impose no-slip on $r = R_0$; then $AR_0 + B/R_0 = 0$, giving $v(r) = (r - R_0^2/r)/(R_0^2 - 1)$. Thus, for $1 \leqslant r \ll R_0$, we have $v(r) \sim -1/r$, the flow due to a virtual point vortex at $r = 0$. In the limit $R_0 \to \infty$, this point-vortex flow extends throughout the fluid tending to zero at infinity, and the fluid exerts a nonzero torque $\mathcal{T}_s = 4\pi\mu[1 + O(R_0^{-2})]$ on the cylinder. This is the scenario that is evident in Watson's [10] remedy (Part II C 3 below), which incorporates the appropriate torque that nullifies the far-field rigid-body rotation.

B. Lubrication approach for the two-cylinder problem

We consider first the situation when the gap between the cylinders is small ($\varepsilon \ll 1$), and lubrication theory is applicable. With the cylinders corotating in the clockwise sense ($\Omega_1 = \Omega_2 = -1$), the lubrication solution for the vertical component of velocity v is very simple: with $v = \pm 1$ on the cylinder boundaries $x = \pm h(y) = \pm(\varepsilon + \frac{1}{2}y^2)$, this solution is the locally Couette flow $v(x, y) = x/h(y)$, and the corresponding stream function satisfying $v(x, y) = -\partial \psi_L/\partial x$ is $\psi_L(x, y) = \frac{1}{2}[h(y)^2 - x^2]/h(y)$. The pressure in this Couette-type flow is evidently uniform in the gap. The streamlines $\psi_L = $ const. are shown in Fig. 15(c) for $\varepsilon = 0.001$. The x component of velocity is

$$u(x, y) = \frac{\partial \psi_L}{\partial y} = y\left[\frac{1}{2} + \frac{2x^2}{(y^2 + 2\varepsilon)^2}\right]. \tag{67}$$

Thus, on the y axis, $u(0, y) = \frac{1}{2}y$; it will turn out that this does correctly represent the flow in the lubrication region $y = \mathrm{O}(\varepsilon^{1/2})$—see Fig. 18(a) below.

The vertical forces on $\mathcal{C}_1$ and $\mathcal{C}_2$ are, respectively,

$$\hat{F}_y = \mp \int_{-\infty}^{\infty} \frac{dy}{h(y)} = \mp\pi(2/\varepsilon)^{1/2}, \tag{68}$$

singular in the limit $\varepsilon \to 0$. In this limit these forces are concentrated very near the points ($\mp\varepsilon, 0$), so the torque on each cylinder about its axis is $\hat{\mathcal{T}} \sim \pi(2/\varepsilon)^{1/2}$. However, the torque relative to the origin (0,0) acting on the pair of cylinders is $\hat{G}(\varepsilon) \sim 2\pi(2\varepsilon)^{1/2}$, vanishing in the limit $\varepsilon \to 0$.

C. Jeffery's paradox and Watson's remedy

1. Jeffery's [2] solution

Using Jeffery's [2] bipolar coordinates [Appendix A and Fig. 10(b)], the solution for corotating cylinders ($\Omega_1 = \Omega_2 = -1$) may be easily obtained. With $\alpha = \cosh^{-1}(1 + \varepsilon)$, the required stream function (an even function of ξ in this case) is found to be

$$\psi_{J2}(x, y) = \frac{\alpha \sinh\alpha \cosh\xi - \xi \sinh\xi \cosh\alpha}{h(\xi, \eta)[\alpha + \cosh\alpha \sinh\alpha]}. \tag{69}$$

Streamlines for the choice $\varepsilon = 1$ ($\alpha = 1.317$) are shown in Fig. 15(a). For $r \gg 1 + \varepsilon$, in polar coordinates and dropping an irrelevant constant, ψ_{J2} has the asymptotic form

$$\psi_{J2}(r, \theta) \sim -\frac{1}{2}\Omega(\alpha)r^2 - \Lambda(\alpha)\cos^2\theta + \mathrm{O}(r^{-2}), \tag{70}$$

where

$$\Omega(\alpha) = -\frac{\alpha}{\alpha + \cosh\alpha \sinh\alpha}, \quad \Lambda(\alpha) = \frac{2\sinh\alpha \cosh\alpha}{\alpha + \sinh\alpha \cosh\alpha}. \tag{71}$$

The first term represents rigid-body rotation with angular velocity $\Omega(\alpha)$, and, in the frame rotating with this angular velocity, the second term represents the instantaneous far-field radial flow of strength $\Lambda(\alpha)$ apparent in Fig. 15(b); "instantaneous" because, in this rotating frame, this radial field rotates in tandem with the two cylinders with angular velocity $-\Omega(\alpha)$. Note that, in the contact limit $\alpha = 0$, $\Omega(0) = -1/2$ and $\Lambda(0) = +1$.

2. Rotating frame solution: Radial quadrupole

Although the solution (70) tends to rigid-body rotation $\Omega(\alpha)$ at infinity, it is nevertheless not without interest. In a frame of reference rotating with this angular velocity, the cylinders 'orbit' with angular velocity $-\Omega(\alpha)$. The torque $\mathcal{T}(\alpha)$ resisting this orbiting is just equal and opposite to the torque $-\mathcal{T}(\alpha)$ on the pair that is generated by their corotation. The net torque experienced by the cylinder pair (and equally the net torque imparted to the fluid) is therefore zero in this situation.
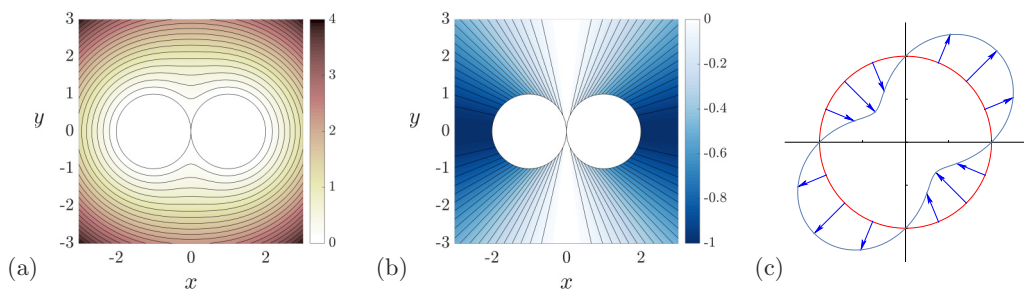
FIG. 16. (a) Streamlines $\psi(r, \theta) = \frac{1}{4}r^2 - \cos^2 \theta = $ const. (in the contact limit $\varepsilon = 0$); (b) streamlines $\psi_Q(r, \theta) = -\cos^2 \theta = $ const; (c) velocity profile for the radial quadrupole, defined in Part II C 2.

In this sense, the situation is quite similar to that of scenario (i) for the model problem in Part II A, when the zero-stress condition is applied on the "remote" cylinder $r = R_0$ (which therefore absorbs zero torque).

Figure 16(a) shows the streamlines $\psi_{J2} = $ const. for the flow (70) in the contact limit $\varepsilon = 0$ ($\alpha = 0$), in the frame of the two cylinders. Figure 16(b) shows the streamlines of the same flow in the frame rotating with angular velocity $\Omega(0) = -\frac{1}{2}$; these streamlines are again purely radial, the normal velocity being nonzero on the cylinders because in this rotating frame the cylinders are orbiting about the origin (as well as still rotating about their respective axes). The streamline pattern of Fig. 16(b) corresponds to the stream function

$$\psi_Q(r, \theta) = -\cos^2 \theta = -\tfrac{1}{2}(1 + \cos 2\theta), \tag{72}$$

a very particular solution of the biharmonic equation. The radial velocity is $u_r(r, \theta) = r^{-1} \sin 2\theta$. In the first quadrant $\{x > 0, \ y > 0\}$ this may be recognized as the low-Reynolds-number limit of the Jeffery-Hamel flow due to a line source of strength $Q = 1$ at the intersection of the plane boundaries $x = 0, \ y = 0$, with no slip on both boundaries ([1], or see, for example, Batchelor [6], Sec. 5.6). In the second quadrant, it represents the same flow but with a line sink $Q = -1$; and in the third and fourth quadrants, it represents again the same flows, source and sink respectively. The total velocity profile going round the circle $r = 1$ is as indicated in Fig. 16(c), outwards in the first and third quadrants, inwards in the second and fourth. It is appropriate to describe this flow as a "radial quadrupole."

3. Watson's remedy

The flow described by the stream function (70) obviously does not satisfy the condition of zero velocity at infinity; this is "Jeffery's paradox" for the corotating situation. Resolution of this paradox was provided by Watson [10], who compared the situation to the case of a single cylinder rotating in an unbounded fluid [scenario (ii) of Part II A], for which the steady flow is that due to a virtual line vortex at the axis of the cylinder. As Watson remarked "it seems implausible that the introduction of a second [corotating] cylinder would change the character of the motion so drastically" (as to replace this asymptotic vortex flow by a rigid-body rotation).

The essential step in Watson's treatment was to introduce a term proportional to $\log[\{(x - c)^2 + y^2\}\{(x + c)^2 + y^2\}]$ in the solution, thereby contributing a vortex ingredient $u_\theta = k/r$ to the velocity at infinity and an associated torque $-4\pi \mu k$ acting on the cylinder pair. It was then necessary to satisfy the no-slip conditions on the two cylinders, and to ensure that the rigid-body term is expunged from the solution. The rather complex details are summarized in Appendix B. We provide some diagrams here that help in the interpretation of Watson's results. Denoting his stream function by $\psi_W(x, y)$, the contours $\psi_W(x, y) = $ const. are shown in Fig. 17(a) for the case $r_1 = 1, \ \varepsilon = 0.1$ (so $\alpha = 0.4436$); the zoom near the origin in Fig. 17(b) shows the expected saddle point at the origin.
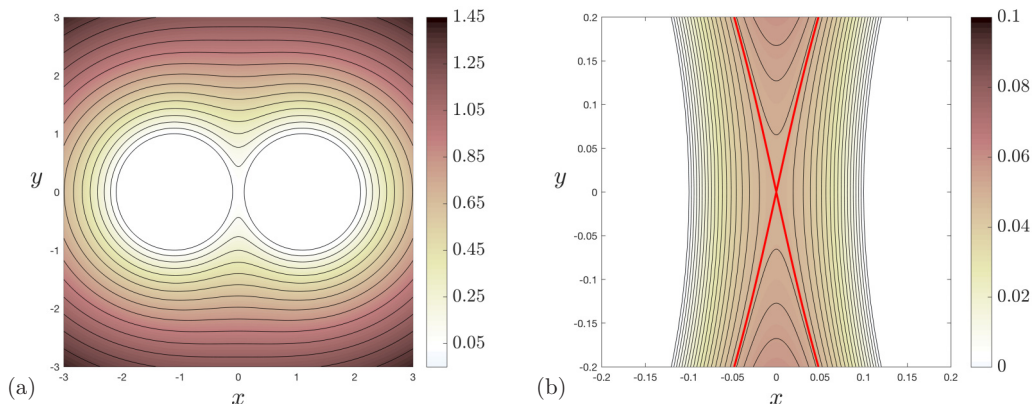
(a) (b)

FIG. 17. (a) Contours $\psi_W(x, y) = $ const. as given by Eq. (B5) in Appendix B, for the situation when $r_1 = 1$, $\varepsilon = 0.1$ (so $\alpha = 0.4436$); (b) zoom of the same near the origin, showing in red the expected saddle point where $\psi_W(0, 0) = 0.0491$.

Figure 18(a) shows the corresponding velocity $u_W(x, y) = \partial \psi_W / \partial y$ on the axis $x = 0$ for $\varepsilon = 0.1$ ($\alpha = 0.4436$, solid black), $\varepsilon = 0.01$ ($\alpha = 0.1413$, solid blue), and $\varepsilon = 0.001$ ($\alpha = 0.04472$, dashed blue); the last two are indistinguishable on the scale shown; the red line, with slope $1/2$, is as given by the lubrication solution (67). Figure 18(b) shows that $|u_W(y)| \sim k |y|^{-1}$ for large $|y|$, as for a point vortex; there is no rigid-body ingredient in this solution. The constant k depends on ε, and may be evaluated numerically as $\lim_{|y| \to \infty} |y \, u_W(y)|$; the function $k(\varepsilon)$ is shown in Fig. 18(c), with the limiting behavior $k(\varepsilon) \sim 1.3734$ as $\varepsilon \downarrow 0$.

Figure 19 shows numerical solutions of the corotating problem with $\varepsilon = 0.01$ for three different conditions on the outer boundary $r = R_0(= 10)$: (a, d) no-slip; (b, e) stress-free; and (c, f) with the boundary condition $v_\theta = -k(\varepsilon)/R_0$ [with $k(0.01)$ derived from the Watson solution—see Fig. 18(c)]. Figure 20 shows corresponding plots of the axial velocity distributions $v(x, 0)$ ($2 < x < 10$) and $u(0, y)$ ($-10 < y < 10$). The Watson solution shows the expected r^{-1} behavior in both plots [as evident also in Fig. 18(b)], and the no-slip solution comes quite close to this.

The stress-free solution is very different; it shows behavior close to rigid-body rotation in the far field, as in the solution originally found by Jeffery [2]. Here again we may compare the situation with the model problem introduced in Part II A: with the stress-free condition [scenario (i)] on the
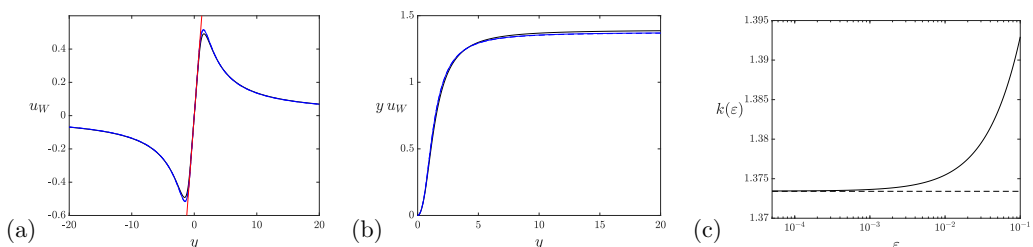

(a) (b) (c)

FIG. 18. (a) Plots of $u_W(0, y)$ for $r_1 = 1$, and $\varepsilon = 0.1$ (solid black), $\varepsilon = 0.01$ (solid blue), $\varepsilon = 0.001$ (dashed blue); the last two curves are indistinguishable on the scale shown. These graphs show the expected behavior $u_W(0, |y|) \sim |y|^{-1}$ for large $|y|$. The red line has slope $1/2$, and correctly represents the flow in the lubrication region $y = O(\varepsilon^{1/2})$; (b) Corresponding plots of $y \, u_W(0, y)$ for positive y, showing that in fact $y \, u_W(0, y) \to k(\varepsilon)$ as $y \to \infty$. (c) The function $k(\varepsilon) = \lim_{|y| \to \infty} |y \, u_W(0, y)|$, which asymptotes to 1.3734 as $\varepsilon \downarrow 0$; this asymptote is shown by the dashed line, which coincides with the level of $\mathcal{T}(0)/4\pi$ as determined by Eq. (75).
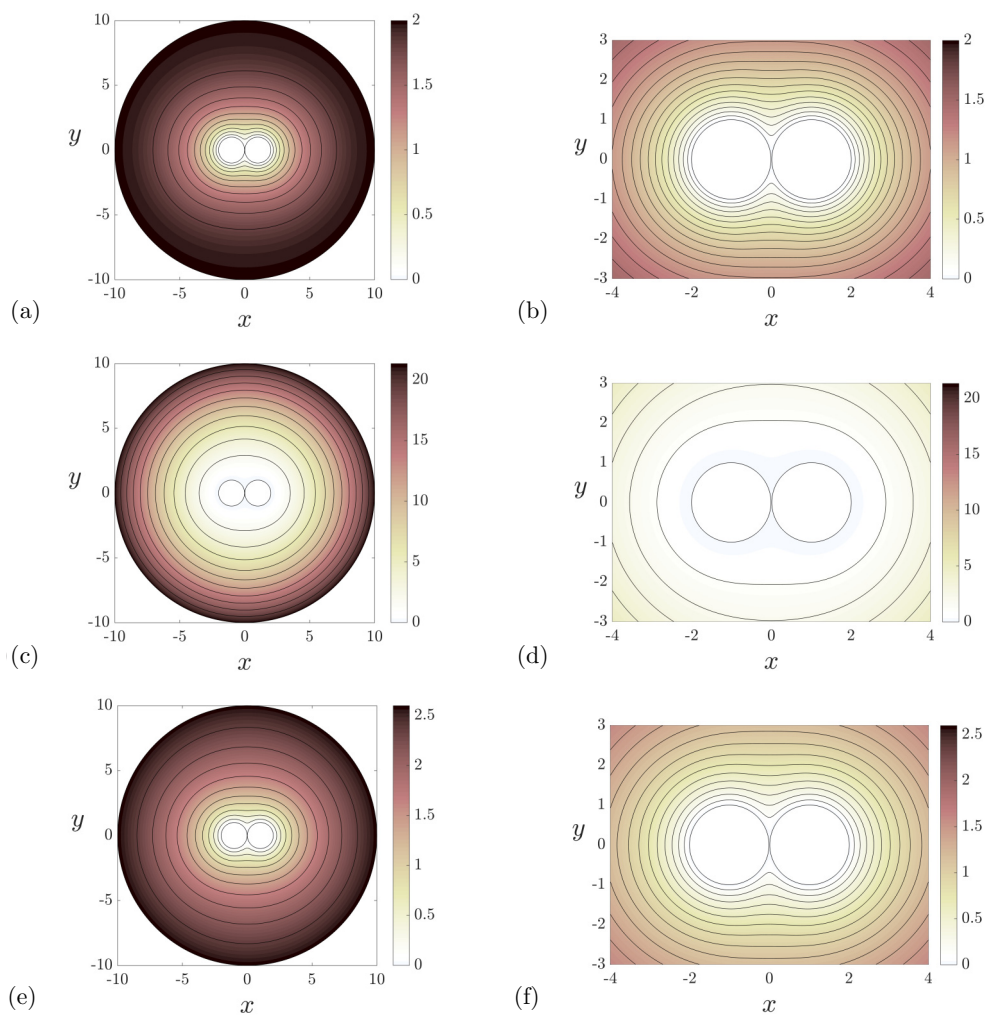
FIG. 19. Streamlines $\psi = $ constant from the numerical solution of the Stokes problem for corotating cylinders with $\varepsilon = 0.01$; the outer boundary condition on $r = R_0$ is either no slip (a), (b); stress-free (c), (d); or (e), (f) with $u_\theta = k(0.01)/R_0$, from Watson [10] and Fig. 18(c).

outer cylinder $r = R_0$; the steady solution in that case is rigid body rotation no matter how large R_0 may be.

4. Torque on cylinder pair

Having expunged the rigid-body term in the general solution, the asymptotic form of $\psi_W(x, y)$ for $r = (x^2 + y^2)^{1/2} \to \infty$ is indeed found to be that of a line vortex

$$\psi_W(x, y) \sim -2K(\alpha) \sinh^2\alpha \log(1/r), \tag{73}$$

where $K(\alpha)$ is the function defined in Appendix B by Eqs. (B1) and (B3); this corresponds to a torque

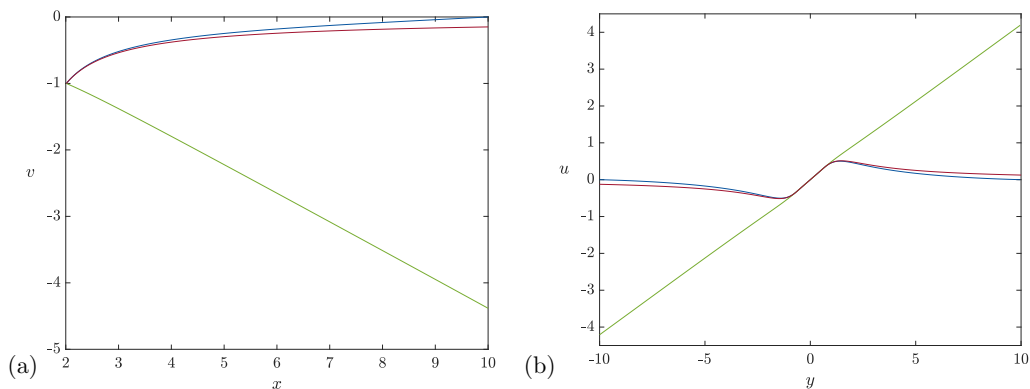$$\hat{\mathcal{T}}(\alpha) = 8\pi K(\alpha) \sinh^2\alpha \tag{74}$$

FIG. 20. Axial velocity distributions corresponding to the streamline plots of Fig. 19; $\varepsilon = 0.01$: (a) $v(x, 0)$ $(2 + \varepsilon < x < 10)$; (b) $u(0, y)$ $(-10 < y < 10)$. The outer boundary condition on $r = R_0$ is either no slip in blue; stress-free in green; or with $u_\theta = k(0.01)/R_0$ in red. The influence of the outer boundary condition is evident: in the no-slip case, the far-field flow is quite close to that of a point vortex ($\sim r^{-1}$ for $r \gg 1$), except near to $r = R_0$ where the no-slip condition is imposed; in the stress-free case, the far field is rigid body rotation ($\sim r$).

exerted by the cylinder pair on the fluid. For small $\varepsilon \sim \frac{1}{2}\alpha^2$, using the asymptotic form (B4) (see Appendix B), this implies that

$$\hat{\mathcal{T}}(\alpha) \sim 8\pi\alpha^2(0.6867\alpha^{-2}) = 17.2587 \quad \text{as } \alpha \to 0; \quad \text{so} \quad \hat{\mathcal{T}}(0)/4\pi = 1.3734 \qquad (75)$$

(cf. $\hat{\mathcal{T}}_s/4\pi = 1$ for a single rotating cylinder). The dashed line in Fig. 18(c) shows that $\hat{\mathcal{T}}(0)/4\pi = 1.3734$ exactly as given by Eq. (75), and the agreement is evidently excellent. Just as for a single cylinder, this torque arises from the stress distribution around the entire boundary of the two cylinders, and the result cannot therefore be obtained from the lubrication theory of Part II B.

In the finite-domain numerical solution, the torque exerted on the fluid jointly by the two inner cylinders must equal the torque absorbed by the outer cylinder $\mathcal{C}_0$. Figure 21 shows the dependence of this torque on R_0 (with the no-slip boundary condition) in the range $8 \leqslant R_0 \leqslant 20$,
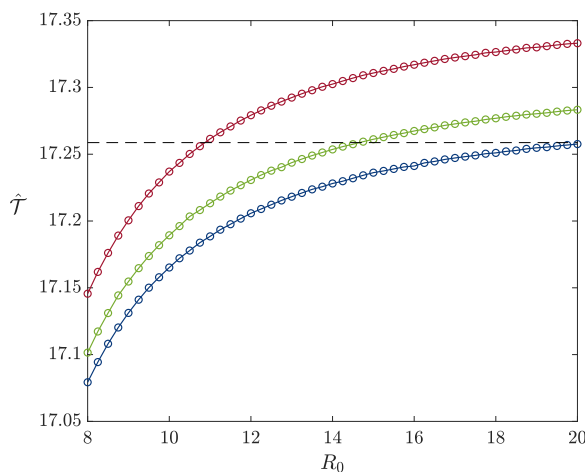

FIG. 21. Torque on the bounding cylinder $\mathcal{C}_0$ (with no-slip boundary condition) as a function of R_0 for $\varepsilon = 0.04$ (red), 0.02 (green), 0.01 (blue). The double limit $R_0 \to \infty$ and $\varepsilon \downarrow 0$ (taken numerically in either order) is needed to approach the asymptotic value 17.2587, marked by the dashed line, as derived in Eq. (75).

for $\varepsilon = 0.04,\ 0.02,$ and 0.01; here, it is the double limiting process $R_0 \to \infty, \varepsilon \downarrow 0$ that shows convergence towards the limit 17.2587, again marked by the dashed line.

DISCUSSION AND CONCLUSIONS

We have here reinvestigated the classical problem of the Stokes flow generated by two parallel rotating circular cylinders of unit radius. We have assumed that the fluid domain $\mathfrak{D}$ is bounded by a cylinder $r = R_0 \gg 1$ on which either no-slip or stress-free boundary conditions can be imposed, and have provided an accurate finite-element numerical treatment of this problem in two cases: counterrotating cylinders in Part I (A–E), and corotating cylinders in Part II (A–C). Note that, insofar as the Stokes problem is linear, the case of arbitrary cylinder rotation rates Ω_1 and Ω_2 is just a linear combination of these two prototypical cases.

Counterrotating cylinders

A model problem exhibiting the same symmetries as the two-cylinder problem was first analyzed in Part I B. This allows asymptotic treatment in an inner regime $1 < r \ll R_0$, and in an outer regime $\{r = kR_0,\ k < 1,\ k = \mathrm{O}(1)\}$ where the influence of inertia forces may be estimated. This shows that, no matter how small the Reynolds number may be, inertia always becomes significant in the outer regime as $[\log R_0]$ increases without limit.

When the gap 2ε between the inner cylinders is small, lubrication theory provides a description of the flow in the gap region that agrees well with the numerical solution. When $\varepsilon \downarrow 0$, two saddle points at $(0, \pm(6\varepsilon)^{1/2})$ move towards the origin. When the cylinders make contact (i.e., when $\varepsilon = 0$), the domain topology changes from triply- to doubly-connected, and the two saddle points convert to two boundary-saddle points. The numerical evidence indicates that when $\varepsilon > 0$ the force exerted on the cylinders tends to zero as $R_0 \to \infty$; this conclusion is consistent with the model calculation of Part I B, the lubrication analysis of Part I C 2, and the analytical solution (for $\varepsilon = 0$) obtained in Part I D. In this case, there is a "contact force" due to the discontinuity of pressure across the point of contact, and we have shown that the total force is continuous down to $\varepsilon = 0$ if and only if this contact force is taken into account.

Based on our results, we may envisage two distinct scenarios for this counterrotating situation when the fluid is unbounded. If the cylinders are free of any external restraining force, then they will move relative to the fluid, ultimately with uniform dimensionless velocity $V [= \frac{1}{2}(1 + \varepsilon)^{-1}]$ in the y direction (just like two parallel line vortices of circulations $\pm\Gamma$ separated by distance $2d$ in an inviscid fluid, which propagate with velocity $V = \Gamma/4\pi d$). In a frame of reference moving with the cylinders, there is thus a uniform streaming velocity $(0, -V)$ at infinity. The ultimate steady state is therefore well described by Jeffery's original solution, the perturbation from the uniform stream being the "torquelet" as given by Eq. (39). The velocity associated with the torquelet is $\mathrm{O}(r^{-2})$ as $r \to \infty$, so that $\mathbf{u}^2 = \mathrm{O}(r^{-4})$. The kinetic energy of the flow in the frame of reference in which the fluid is at rest at infinity is therefore finite, and this flow could therefore be generated from a state of rest in a finite time.

If however, the cylinders are constrained in such a way that their axes are fixed as they rotate, then the situation is quite different. If in this situation the rotation is started impulsively at $t = 0$, then a low Reynolds number flow will develop, as analyzed by Ueda *et al.* [15]. This flow incorporates both stokeslet and uniform-streaming ingredients, but extends only over a range $r \lesssim \mathrm{Re}^{-1} \log[\mathrm{Re}^{-1}]$, limited by inertia effects. The cylinders must then experience a net force $\hat{F}_y$ in the limit $\mathrm{Re} \to 0$ that we estimate to be $\hat{F}_y \sim 1/\log[\mathrm{Re}^{-1} \log[\mathrm{Re}^{-1}]]$. The problem of matching this Stokes flow to an outer solution of the full Navier-Stokes equations remains open.

Corotating cylinders

Again in this case, an elementary model problem is presented in Part II A, for which the boundary condition on the outer cylinder $r = R_0$ may be stress-free or no-slip. For the two-cylinder corotating

problem, these alternatives correspond to two quite distinct scenarios which emerge from our analysis, We have provided a finite-element numerical solution for both scenarios when $R_0 \gg 1$. Lubrication theory describes well the highly sheared flow in the narrow gap when $\varepsilon \ll 1$, and good agreement is achieved with the full numerical solution.

In the first scenario, a zero-stress condition is applied on $r = R_0$, and the flow tends in the far field to rigid-body rotation with angular velocity $\Omega(\alpha)$, where $\alpha = \cosh^{-1}(1 + \varepsilon)$; there is in this situation zero net torque on the cylinder pair. In an unbounded fluid, this is essentially the solution of Jeffery [2]. In a frame of reference rotating with the fluid at infinity the cylinders orbit with angular velocity $-\Omega(\alpha)$, and this is the behavior if their axes are unconstrained. In this rotating frame, the fluid velocity is identified as a "radial quadrupole."

In the second scenario, the cylinder axes are supposed be held fixed by external constraints. Their corotation about these fixed axes then generates a localized torque on the fluid and so a vortex-like flow $u_\theta \sim k(\varepsilon)r^{-1}$ in the far field. (This is approximately realized numerically by imposing a no-slip condition on $r = R_0$.) There is also an internally driven rigid-body rotation, but, following Watson [10], this is nullified by suitable choice of the strength of the virtual vortex [thus in effect determining the function $k(\varepsilon)$], so that the resulting velocity tends to zero for large r thus resolving Jeffery's paradox in this case. We have extended and refined Watson's analysis to reveal the behavior as $\varepsilon \downarrow 0$; in this limit we have shown that the torque $\hat{\mathcal{T}}$ on the cylinder pair asymptotes to the value 17.2587.

ACKNOWLEDGMENTS

APPENDIX A: ASYMPTOTIC BEHAVIOR OF JEFFERY'S [2] SOLUTION

Jeffery [2] used bipolar coordinates defined by a conformal mapping $\xi + i\eta = \log \frac{x+iy+c}{x+iy-c}$, so that

$$\xi(x, y) = \frac{1}{2} \log \frac{(x + c)^2 + y^2}{(x - c)^2 + y^2}, \quad \eta(x, y) = \tan^{-1}\left[\frac{x+c}{y}\right] - \tan^{-1}\left[\frac{x-c}{y}\right]. \tag{A1}$$

The scale factor for this mapping is $h(\xi, \eta) = |d\zeta/dz| = (\cosh \xi - \cos \eta)/c$. The contours $\xi(x, y) = $ const., $\eta(x, y) = $ const. are shown in Fig. 10(b). The contour $\xi = \alpha$ is a circle with center at $(c_1, 0)$ where $c_1 = c \coth \alpha$, and radius $r_1 = c \operatorname{cosech}|\alpha|$. If we fix $r_1 = 1$, then $c = \sinh |\alpha|$, and the separation of the two cylinders is (as before) 2ε, where now $\varepsilon = \cosh \alpha - 1$, i.e., $\alpha = \cosh^{-1}(1 + \varepsilon)$. The boundaries $\mathcal{C}_{1,2}$ are taken to be $\xi = \mp\alpha$ with $\alpha > 0$, and the fluid domain is $\mathfrak{D} : \{0 \leqslant |\xi| < \alpha, -\pi < \eta < \pi\}$.

With this notation, Jeffery ([2], p. 173) found the stream function for the counterrotating situation in the form

$$\psi_J(x, y) = [h(\xi, \eta)]^{-1}[b_0 \xi (\cosh \xi - \cos \eta) + c_0 \sinh \xi + c_1 \sinh 2\xi \cos \eta], \tag{A2}$$

where the constants b_0, c_0 and c_1 take values determined by the boundary conditions

$$b_0 = -\frac{\cosh 2\alpha}{2 \cosh \alpha \sinh^2 \alpha}, \quad c_0 = \frac{\cosh \alpha}{2 \sinh^2 \alpha}, \quad c_1 = -\frac{1}{4 \cosh \alpha \sinh^2 \alpha}. \tag{A3}$$

The stream function ψ_J then takes the asymptotic form (for $r = (x^2 + y^2)^{1/2} \gg 1$)

$$\psi_J(x, y) \sim \frac{x}{2 \cosh \alpha} - \frac{2x[x^2 + (x^2 + y^2) \sinh^2 \alpha]}{\cosh \alpha (x^2 + y^2)^2} + \mathrm{O}(r^{-3}), \tag{A4}$$
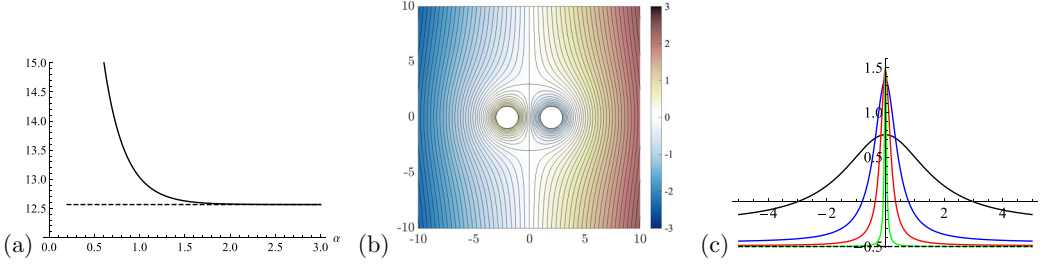
FIG. 22. (a) The function $\hat{\mathcal{T}}_2(\alpha)$ [cf. Fig. 14(a)] showing the large-α asymptote (dashed) at the level $4\pi \approx$ 12.566; (b) streamlines $\psi_J(x, y, \alpha) = $ const. as given by Eq. (A2), for the choice $\varepsilon = 1$ ($\alpha = 1.317$); for this choice, the saddle points are at $y = \pm 3$ and the flow asymptotes to the uniform stream $(-\frac{1}{4}, 0)$ as $r \to \infty$; (c) the velocity $v_J(0, y)$ for $\varepsilon = 1$ (black), 0.1 (blue), 0.2 (red), and 0.001 (green); in the limit $\varepsilon = 0$, the asymptotic uniform stream is $(-\frac{1}{2}, 0)$, as shown by the dashed line.

or equivalently in polar coordinates

$$\psi_J(r, \theta) \sim \frac{r \cos \theta}{2 \cosh \alpha} - \frac{(4 \cosh^2 \alpha - 1) \cos \theta + \cos 3\theta}{2r \cosh \alpha} + \mathrm{O}(r^{-3}), \tag{A5}$$

giving Eq. (39) in the limit $\alpha = 0$. The leading term in Eq. (A4) represents a uniform stream $(0, -\frac{1}{2} \operatorname{sech} \alpha) = [0, -\frac{1}{2}(1+\varepsilon)^{-1}]$ as found by Jeffery, and the second term, of order r^{-1}, which has not been previously identified, represents a torquelet, whose strength, noting the structure of Eq. (A5), may be defined as, say,

$$\mu_{\mathcal{T}} = \pi(4 \cosh^2 \alpha - 1) \operatorname{sech} \alpha = d(\alpha) \hat{\mathcal{T}}_2(\alpha)/2. \tag{A6}$$

Here, $d(\alpha)$ is the separation of virtual point torques of magnitude $\pm \hat{\mathcal{T}}_2(\alpha)$ needed to give precisely this torquelet strength. The flattening of the streamlines evident in Fig. 12(a) decreases as α increases, i.e., as the separation of the cylinders is increased, with corresponding decrease of their mutual interaction. Figure 22(a) again shows the function $\hat{\mathcal{T}}_2(\alpha)$ computed from Jeffery's solution (A2), but here in the range $\alpha \gtrsim 0.5$, ($\varepsilon \gtrsim 0.13$); this shows rapid approach to the asymptotic level 4π, this limit being quite accurately reached for $\alpha \gtrsim 2$, i.e., for $\varepsilon = \cosh \alpha - 1 \gtrsim 2.75$. The separation $d(\alpha)$ then asymptotes to $2 \cosh \alpha = 2(1 + \varepsilon)$, the distance between the centres of $\mathcal{C}_1$ and $\mathcal{C}_2$, as might be expected.

At the other extreme $\alpha \to 0$, as we have seen from Fig. 14(a), $\hat{\mathcal{T}}_2(\alpha) \sim 2\pi/\alpha$, so that in this limit the separation $d(\alpha)$ is given by $d(\alpha) \sim 6\pi/\hat{\mathcal{T}}_2(\alpha) \sim 3\alpha \sim 3(2\varepsilon)^{1/2}$, as stated in Part II C 4. For $\alpha \sim (2\varepsilon)^{1/2} \ll 1$ (and $r \gg \varepsilon^{1/2}$, i.e., outside the lubrication zone), the solution (A2) may be expanded in powers of ε; in polar coordinates, at leading order this gives

$$\psi_J(r, \theta) = \tfrac{1}{2} r \cos \theta - \tfrac{1}{2} r^{-1}(3 \cos \theta + \cos 3\theta) + \mathrm{O}(\varepsilon), \tag{A7}$$

recovering the result (39) when $\varepsilon = 0$.

At the intermediate value $\varepsilon = 1$ (so $\alpha = 1.317$), the streamlines $\psi_J = $ const. are as shown in Fig. 22(b). For this choice of ε, the saddle points are at $y = \pm 3$ and the flow settles to the uniform stream $(0, -\frac{1}{4})$ as $r \to \infty$. Moreover, $\hat{\mathcal{T}}_2(1.317) = 12.70$ and d evaluates to 3.71, somewhat less than $4 [= 2(1 + \varepsilon)]$, the distance between the centres of $\mathcal{C}_1$ and $\mathcal{C}_2$. This is to be expected, because the tangential stress $\hat{\tau}(\phi)$ on $\mathcal{C}_2$ becomes more pronounced near the gap location $\phi = \pm \pi$ as ε decreases (and similarly of course for $\mathcal{C}_1$).

Figure 22(c) shows the velocity $v_J(0, y)$ for the four choices $\varepsilon = 1$, 0.2, 0.1 and 0.001. For large $|y|$,

$$v_J(0, y) \sim -\frac{1}{2 \cosh \alpha} + \frac{2 \sinh^2 \alpha}{\cosh \alpha} y^{-2} + \mathrm{O}(y^{-4}) = -\frac{1}{2(1 + \varepsilon)} + \frac{2\varepsilon(2 + \varepsilon)}{(1 + \varepsilon)} y^{-2} + \mathrm{O}(y^{-4}), \tag{A8}$$

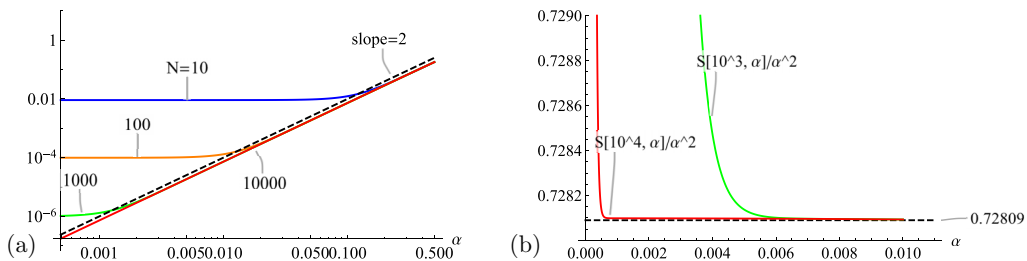the leading term giving the streaming velocity $[0, -\frac{1}{2}(1 + \varepsilon)^{-1}]$ as $|y| \to \infty$.

FIG. 23. (a) Log-log plots of the functions $S[N, \alpha]$ for $N = 10, 10^2, 10^3, 10^4$, indicating that $S[N, \alpha] \sim k\alpha^2$ over a range of α that extends towards $\alpha = 0$ with increasing N; (b) plots of $\alpha^{-2}S[N, \alpha]$ for $N = 10^3, 10^4$, indicating that $k \approx 0.7281$.

APPENDIX B: ASYMPTOTIC ANALYSIS OF WATSON'S [10] SOLUTION

Watson's [10] solution of the corotating problem involved the function

$$S(\alpha) = \frac{1}{2} + \frac{\alpha \sinh^2 \alpha \tanh \alpha}{\alpha + \sinh \alpha \cosh \alpha} - 4 \sum_{n=2}^{\infty} \frac{\sinh \alpha(\sinh \alpha + n \cosh \alpha) + n\,e^{-n\alpha} \sinh n\alpha}{(n^2 - 1)(n \sinh 2\alpha + \sinh 2n\alpha)}, \qquad \text{(B1)}$$

where α is related to the gap parameter ε (as in Appendix A) by $\alpha = \cosh^{-1}(1 + \varepsilon)$. The convergence of the sum here is an issue of immediate concern. For any fixed $\alpha > 0$, the coefficient in the nth term of the sum is proportional to $n^{-1} e^{-2n\alpha}$ for large n, so that convergence is assured. However, as $\varepsilon \to 0$, i.e., $\alpha \to 0$, more and more terms of the series must be retained to get any prescribed level of accuracy. Defining $S[N, \alpha]$ as the function (B1) when the summation is truncated at $n = N$, Fig. 23(a) shows log-log plots of $S[N, \alpha]$, for $N = 10, 10^2, 10^3, 10^4$. The dashed line has slope 2, indicating that, as $N \to \infty$, $S[N, \alpha] \sim k\alpha^2$ for some constant k. Figure 23(b) shows the functions $S[10^3, \alpha]/\alpha^2$ and $S[10^4, \alpha]/\alpha^2$, indicating that $k = 0.7281$ to good approximation. As expected, this behavior breaks down when α is too small ($\lesssim 0.001$ when $N = 10^4$), but it nevertheless indicates that the limiting function $S(\alpha)$ has an asymptotic behavior

$$S(\alpha) \sim 0.7281\,\alpha^2 \quad \text{as } \alpha \to 0. \qquad \text{(B2)}$$

A second function $K(\alpha)$ is then defined by

$$K(\alpha) = \frac{\alpha}{S(\alpha)(\alpha + \sinh \alpha \cosh \alpha)}, \qquad \text{(B3)}$$

with asymptotic behavior that follows from Eq. (B2),

$$K(\alpha) \sim 0.6867\alpha^{-2} \quad \text{as } \alpha \to 0 \qquad \text{(B4)}$$

(and actually $\alpha^2 K(\alpha) < 0.6868$ for all $\alpha > 0$).

In view of the symmetry, we may restrict attention to the half-space $x \geqslant 0$, and to the fluid region $0 \leqslant \xi < \alpha$. With $\xi(x, y)$, $\eta(x, y)$ and $h(\xi, \eta)$ as defined in Appendix A of Part 1, Watson's stream function is given by

$$\psi_W(x, y) = -\frac{\sinh \alpha \ \phi[\xi(x, y), \eta(x, y)]}{h[\xi(x, y), \eta(x, y)]}, \qquad \text{(B5)}$$

where $\phi(\xi, \eta)$ has the Fourier series representation

$$\phi(\xi, \eta) = K(\alpha)(\cosh \xi - \cos \eta) \log(2 \cosh \xi - 2 \cos \eta) + a_0(\alpha) \cosh \xi + b_0(\alpha)\xi \sinh \xi$$

$$+ \sum_{n=1}^{\infty} [a_n(\alpha) \cosh(n+1)\xi + b_n(\alpha) \cosh(n-1)\xi] \cos n\eta. \qquad \text{(B6)}$$

Here the coefficients are given by

$$a_0(\alpha) = -\frac{\alpha + K(\alpha)(\alpha + \alpha^2 + e^{-\alpha}\sinh\alpha)}{\alpha + \sinh\alpha\cosh\alpha}, \quad b_0(\alpha) = \frac{\coth\alpha - K(\alpha)\sinh^2\alpha}{\alpha + \sinh\alpha\cosh\alpha}, \quad (B7)$$

$$a_1(\alpha) = \frac{1}{2}K(\alpha)e^{-\alpha}\mathrm{sech}\,\alpha, \quad b_1(\alpha) = K(\alpha)\left(1 + \alpha - \frac{1}{2}\tanh\alpha\right), \quad (B8)$$

and, for $n \geqslant 2$,

$$a_n(\alpha) = \frac{2K(\alpha)(ne^{-\alpha}\sinh\alpha + e^{-n\alpha}\sinh n\alpha)}{n(n+1)(\sinh 2n\alpha + n\sinh 2\alpha)}, \quad b_n(\alpha) = -\frac{2K(\alpha)(ne^{\alpha}\sinh\alpha + e^{-n\alpha}\sinh n\alpha)}{n(n-1)(\sinh 2n\alpha + n\sinh 2\alpha)}.$$
$$(B9)$$

Again, for any fixed $\alpha > 0$, these coefficients have the asymptotic behavior

$$a_n(\alpha) \sim \frac{4K(\alpha)e^{-\alpha}\sinh\alpha}{n\,e^{2n\alpha}}, \quad b_n(\alpha) \sim -\frac{4K(\alpha)e^{\alpha}\sinh\alpha}{n\,e^{2n\alpha}} \quad \text{as } n \to \infty, \quad (B10)$$

so that the coefficient of $\cos n\eta$ in Eq. (B6) has the behavior

$$[a_n(\alpha)\cosh(n+1)\xi + b_n(\alpha)\cosh(n-1)\xi] \sim \frac{4K(\alpha)}{n\,e^{(n-1)(\alpha-\xi)}\,e^{n\alpha}} \quad \text{as } n \to \infty. \quad (B11)$$

The series in Eq. (B6) therefore converges exponentially rapidly for $0 \leqslant \xi \leqslant \alpha$, and may again be evaluated to good approximation if terminated at $n = N$ provided N is appropriately chosen in relation to α. Since $\alpha \sim (2\varepsilon)^{1/2}$ for $\varepsilon \ll 1$, we therefore need $N \gg (2\varepsilon)^{-1/2}$. When $\varepsilon = 0.1$, this requirement is simply $N \gg 1$; we actually ran to $N = 1000$ in constructing Figs. 17 and 18, thus providing extreme accuracy. If $N = 10$ is used instead, then the resulting figures are just as good at this value of ε, but if ε is reduced, then N must be correspondingly increased to maintain accuracy.

The definitions (B7)–(B9) ensure that the impermeability and no-slip conditions are satisfied on the corotating cylinders $\xi = \pm\alpha$. These conditions are

$$\phi(\alpha, \eta) = 0 \quad \text{and} \quad \sinh\alpha\,\frac{\partial\phi}{\partial\xi}\bigg|_{\xi=\alpha} = 1 \quad \text{for } -\pi < \eta \leqslant \pi. \quad (B12)$$

Normalizing $\phi(\alpha, \eta)$ by its value at $\xi = 0$, $\eta = \pi$ (corresponding to the point $x = 0$, $y = 0$), Fig. 24 shows $\phi(\alpha, \eta)/\phi(0, \pi)$ and $\sinh\alpha\,\partial\phi/\partial\xi|_{\xi=\alpha}$, evaluated for two cases: $\varepsilon = 0.1$ ($\alpha = 0.4583$) truncating the series at $N = 10$; and $\varepsilon = 0.01$ ($\alpha = 0.1413$) truncating the series at $N = 20$. The conditions are satisfied to well within 0.2% and 2% accuracy respectively at these levels of truncation. As ε is further decreased, N must be correspondingly increased to retain accuracy.

The coefficient of the "rigid-body" term in the solution as $r \to \infty$ (i.e., as $\xi^2 + \eta^2 \to 0$) is proportional to

$$R(\alpha) \equiv a_0(\alpha) + \sum_{n=1}^{\infty}[a_n(\alpha) + b_n(\alpha)], \quad (B13)$$

and it is the condition $R(\alpha) \equiv 0$ that actually determines the function $K(\alpha)$ [through Eqs. (B1) and (B3)]. Provided the same N is chosen in Eqs. (B1) and (B6), this condition is actually identically satisfied for any N, as may be verified with some effort.

APPENDIX C: NUMERICAL MODELING

Finite elements were used to determine the Stokes flow in the triply connected fluid domain $\mathfrak{D}$ between the inner cylinders $\mathcal{C}_{1,2}$ and the outer cylinder $\mathcal{C}_0$. On $\mathcal{C}_{1,2}$, the boundary conditions were "no-slip," i.e., $\mathbf{u}|_{\{1,2\}} = \omega_{\{1,2\}}\,\mathbf{e}_z \wedge \mathbf{n}$ (with unit outward normal $\mathbf{n}$), and on $\mathcal{C}_0$, the no-slip condition $\mathbf{u}|_0 = 0$ was also imposed. These are "essential" boundary conditions in finite-element terms, in that they are imposed explicitly on the solution $\mathbf{u}$.
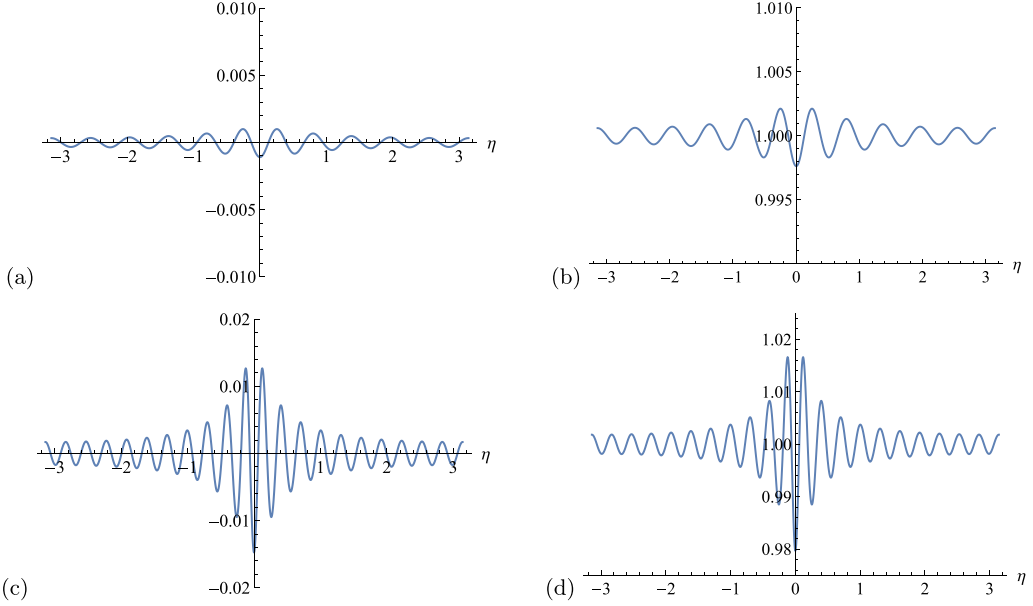
FIG. 24. Verification of the impermeability and no-slip conditions (B12) on $\xi = \alpha$; (a), (b) $\phi(\alpha, \eta)/\phi(0, \pi)$ and $\sinh \alpha \, \partial \phi / \partial \xi |_{\xi = \alpha}$; $\alpha = 0.4583, N = 10, \phi(0, \pi) = -0.4681$; (c), (d) the same for $\alpha = 0.1413, N = 20, \phi(0, \pi) = -0.4972$.

The finite-element formulation involves writing the equations in variational form; it is then required to find $\mathbf{u}$ in $\mathcal{W}_{\mathrm{bc}}$ and $\hat{p}$ in $\mathcal{Q}$ such that

$$2 \int_{\mathfrak{D}} \mathbf{e}(\mathbf{u}) : \mathbf{e}(\mathbf{w}) \, d\mathbf{x} - \int_{\mathfrak{D}} \hat{p} \, \nabla \cdot \mathbf{w} \, d\mathbf{x} = 0, \quad \forall \mathbf{w} \in \mathcal{W}_0, \tag{C1a}$$

$$\int_{\mathfrak{D}} q \, \nabla \cdot \mathbf{u} \, d\mathbf{x} = 0, \quad \forall q \in \mathcal{Q}, \tag{C1b}$$

where $\mathbf{e}(\mathbf{u})$ is the rate-of-strain tensor, with cartesian components e_{ij}, and $\mathcal{W}_{\mathrm{bc}}$, $\mathcal{W}_0$, and $\mathcal{Q}$ are suitably defined function spaces,

$$\mathcal{W}_{\mathrm{bc}} = \{\mathbf{w} \in [H^1(\mathfrak{D})]^2 \, : \, \mathbf{w}|_{\{0,1,2\}} = \mathbf{u}|_{\{0,1,2\}}\}, \tag{C2a}$$

$$\mathcal{W}_0 = \{\mathbf{w} \in [H^1(\mathfrak{D})]^2 \, : \, \mathbf{w}|_{\{0,1,2\}} = 0\} \quad \text{and} \quad \mathcal{Q} = \{q \in L^2(\mathfrak{D}) \, : \, \langle q \rangle_{\mathfrak{D}} = 0\}. \tag{C2b}$$

$\mathcal{Q}$ consists of functions with zero mean on $\mathfrak{D}$; this allows for the fact that the pressure is determined only up to an arbitrary constant. These function spaces are then approximated with discrete spaces, here by a triangular mesh, and with quadratic elements for the velocity and affine elements for pressure. The resulting system was solved using *FreeFem* $++$ [22].

Computing the stream function is not straightforward since the domain is not simply connected; ψ can be set to zero on only one boundary: we set $\psi|_0 = 0$ on $\mathcal{C}_0$. The value of ψ on $\mathcal{C}_1$ and $\mathcal{C}_2$ is not known *a priori*. These missing boundary conditions can however be recovered from the solution of Eq. (C1) as

$$\psi_{\{1,2\}} = \pm \frac{1}{2} Q \quad \text{with } Q = \int_{-\varepsilon}^{\varepsilon} v(x, 0) \, dx, \tag{C3}$$

and by solving

$$\nabla^2 \psi = -(\nabla \wedge \mathbf{u}) \cdot \mathbf{e}_z \quad \text{with} \quad \psi|_{\{0,1,2\}} = \psi_{\{0,1,2\}}, \tag{C4}$$

or equivalently (but with higher-order shape functions) by solving $\nabla^4 \psi = 0$ with the additional boundary conditions $\mathbf{n} \cdot \nabla \psi|_{\{1,2\}} = \mp 1$, respectively.

Some simulations using a stress-free outer boundary were also carried out for the corotating case. With $\mathbf{n}$ and $\mathbf{t}$ unit normal and tangent vectors on $\mathcal{C}_0$, the boundary conditions become

$$\mathbf{n} \cdot \mathbf{u}|_0 = 0, \quad \mathbf{n} \cdot \mathbf{e}(\mathbf{u}) \cdot \mathbf{t}|_0 = 0, \quad \text{on} \quad \mathcal{C}_0, \tag{C5}$$

and it is in general a nontrivial matter to implement these conditions. In writing the variational form for this problem, the conditions on $\mathbf{w}|_{\{0\}}$ must be relaxed for both $\mathcal{W}_{\text{bc}}$ and $\mathcal{W}_0$. Since the full rate-of-strain tensor $\mathbf{e}$ was retained in the numerical formulation, the integration by parts that yields Eq. (C1a) remains valid as stated with the boundary conditions (C5). The impenetrability condition is "essential," and needs to be imposed strongly by a penalization of the minimization problem (C1) with

$$\oint_{\mathcal{C}_0} (\mathbf{n} \cdot \mathbf{u})(\mathbf{n} \cdot \mathbf{w}) \, ds, \tag{C6}$$

where s is arclength on $\mathcal{C}_0$, whereas the condition $\mathbf{n} \cdot \mathbf{e}(\mathbf{u}) \cdot \mathbf{t}|_0 = 0$ is "natural," following from the weak form (C1).

Finally, to resolve variables with sufficient accuracy over the full range of scales $[\varepsilon, R_0]$, and to reduce matrix sizes, an Uzawa splitting was employed in our largest simulations.

---

[1] G. B. Jeffery, The two-dimensional steady flow of a viscous fluid, London, Edinburgh, Dublin Philos. Mag. J. Sci. **29**, 455 (1915).

[2] G. B. Jeffery, The rotation of two circular cylinders in a viscous fluid, Proc. R. Soc. A **101**, 169 (1922).

[3] E. Lauga, *The Fluid Dynamics of Cell Motility* (Cambridge University Press, Cambridge, UK, 2020).

[4] D. Nie, Y. Ying, G. Guan, J. Lin, and Z. Ouyang, Two-dimensional study on the motion and interactions of squirmers under gravity in a vertical channel, J. Fluid Mech. **960**, A31 (2023).

[5] H. Lamb, *Hydrodynamics* (Cambridge University Press, Cambridge, UK, 1932).

[6] G. K. Batchelor, *An Introduction to Fluid Dynamics* (Cambridge University Press, Cambridge, UK, 1967).

[7] I. Proudman and J. R. A. Pearson, Expansions at small Reynolds numbers for the flow past a sphere and a circular cylinder, J. Fluid Mech. **2**, 237 (1957).

[8] See Supplemental Material at http://link.aps.org/supplemental/10.1103/PhysRevFluids.9.044102 for the case of overlapping cylinders (i.e., $\varepsilon < 0$).

[9] C. P. Hills, Flow patterns in a two-roll mill, Q. J. Mech. Appl. Math. **55**, 273 (2002).

[10] E. J. Watson, The rotation of two circular cylinders in a viscous fluid, Mathematika **42**, 105 (1995).

[11] W. G. Bickley, LXXIII. The plane jet, London, Edinburgh, Dublin Philos. Mag. J. Sci. **23**, 727 (1937).

[12] J. M. Dorrepaal, M. E. O'Neill, and K. B. Ranger, Two-dimensional Stokes flows with cylinders and line singularities, Mathematika **31**, 65 (1984).

[13] L. Elliott, D. B. Ingham, and T. B. A. El Bashir, The solution of a paradoxical slow flow problem using a boundary element method, Eng. Anal. Bound. Elem. **15**, 29 (1995).

[14] L. Elliott, D. B. Ingham, and T. B. A. El Bashir, Stokes flow past two circular cylinders using a boundary element method, Comput. Fluids **24**, 787 (1995).

[15] Y. Ueda, A. Sellier, T. Kida, and M. Nakanishi, On the low-Reynolds-number flow about two rotating circular cylinders, J. Fluid Mech. **495**, 255 (2003).

[16] M. J. Lighthill, On the squirming motion of nearly spherical deformable bodies through liquids at very small Reynolds numbers, Commun. Pure Appl. Math. **5**, 109 (1952).

[17] E. Lauga and T. R. Powers, The hydrodynamics of swimming microorganisms, Rep. Prog. Phys. **72**, 096601 (2009).

[18] H. Hertz, Uber die Berührung fester elastischer Körper (On the contact of elastic solids), J. Reine Angew. Math. **1882**, 156 (1882).

[19] B. Tavakol, G. Froehlicher, D. P. Holmes, and H. A. Stone, Extended lubrication theory: Improved estimates of flow in channels with variable geometry, Proc. R. Soc. A **473**, 20170234 (2017).

[20] G. Schubert, Viscous flow near a cusped corner, J. Fluid Mech. **27**, 647 (1967).

[21] E. Lauga and S. Michelin, Stresslets induced by active swimmers, Phys. Rev. Lett. **117**, 148001 (2016).

[22] F. Hecht, New development in *FreeFem* ++, J. Numer. Math. **20**, 251 (2012).